https://doi.org/10.5194/egusphere-2026-2517
Preprint. Discussion started: 11 June 2026

NUKLEUS - A first kilometer-scale convection-permitting multi-model climate ensemble for Germany: Characteristics of the historical simulations 1961–1990

Christoph Braun[1,★], Florian Ehmele[1,★], Christian Beier[2], Edgar Fabián Espitia-Sarmiento[3,6], Hendrik Feldmann[1], Thomas Frisius[4], Beate Geyer[5], Marie Hundhausen[1], Klaus Keuler[2], Jürg Luterbacher[3], Kevin Sieck[5], Katja Trachte[2], Elena Xoplaki[3,7], and Joaquim G. Pinto[1]

[1]Institute of Meteorology and Climate Research, Troposphere Research (IMKTRO), Karlsruhe Institute of Technology (KIT), Karlsruhe, Germany
[2]Chair of Atmospheric Processes, Brandenburg University of Technology (BTU) Cottbus-Senftenberg, Cottbus, Germany
[3]Department of Geography, Justus Liebig University (JLU) Giessen, Giessen, Germany
[4]Climate Service Center Germany (GERICS), Helmholtz-Zentrum Hereon, Hamburg, Germany
[5]Institute of Coastal Systems - Analysis and Modeling, Helmholtz-Zentrum Hereon, Geesthacht, Germany
[6]now at: Leibniz Supercomputing Center, Environmental Computing, Garching, Germany
[7]now at: CMCC Foundation – Euro-Mediterranean Center on Climate Change, Bologna, Italy
★These authors contributed equally to this work.

Correspondence: Christoph Braun (christoph.braun@kit.edu) and Florian Ehmele (florian.ehmele@kit.edu)

Abstract. This study presents the evaluation of the historical reference simulations (1961–1990) of the NUKLEUS ensemble, the first kilometer-scale convection-permitting multi-model climate ensemble for Germany. The main goal is to examine to what extent these high-resolution simulations can provide high-quality and actionable information for climate adaptation measures in Germany. The NUKLEUS ensemble comprises nine members, generated by dynamically downscaling three global climate models from the Coupled Model Intercomparison Project phase 6 (CMIP6) with three regional climate models to a 3 km grid over a Central European domain. The evaluation focuses on the spatio-temporal and statistical representation of basic meteorological variables (temperature, wind speed, and precipitation) and derived application-relevant climate indices compared to reanalyses and observation-based data sets. The analyses are performed for Germany and six pilot regions representing diverse climatic and physiographic settings. The results reveal that the ensemble overall exhibits moderate biases with temperature and precipitation generally showing high distributional skill. Only few simulations exhibit strong warm biases, particularly during summer, while all simulations exhibit a wet bias throughout the year, except local dry biases during summer in individual members. Wind biases are more heterogeneous, particularly due to reference data constraints over complex terrain. Percentile-based climate indices are well reproduced, while fixed-threshold indices show systematic deviations. A comparison with previous regional climate model ensembles highlights the added value of the here-chosen multi-model approach. With regard to downstream applications, a quantile (delta) mapping bias correction is applied to daily precipitation totals and daily mean, minimum, and maximum temperature, which removes climatological biases and markedly improves threshold-based indices. The paper also demonstrates important limitations of this bias correction approach for event-based applications, showing that it may disrupt spatial coherence and introduce spurious spatial gradients in precipitation fields, which can affect the

https://doi.org/10.5194/egusphere-2026-2517
Preprint. Discussion started: 11 June 2026

characterization of extreme precipitation events. Overall, the presented analyses support the use of the NUKLEUS ensemble as a high-resolution basis for regional climate and impact studies, while underlining that application-oriented post-processing and validation should be tailored to the target variable and use case.

1 Introduction

Current international modeling initiatives, such as the coupled model intercomparison project phase 6 (CMIP6) and the European branch of the world climate research program's (WCRP) coordinated regional downscaling experiments (EURO-CORDEX), have substantially advanced our understanding of global and regional climate dynamics. It provided ensembles of global climate model (GCM) simulations (Eyring et al., 2016) and dynamically downscaled regional climate model (RCM) products (Jacob et al., 2014). One insight is that ongoing climate change is already altering the frequency and intensity of extreme weather events, with the largest impacts at regional to local scales (Masson-Delmotte et al., 2021). Hence, an immediate and effective adaptation to changing climatic conditions is crucial (Measham et al., 2011; Pörtner et al., 2023; Fünfgeld et al., 2023).

In recent years, Germany experienced multiple extreme events, such as the extreme drought of 2018 (Rousi et al., 2023) and the catastrophic Ahr Valley flood in 2021 (Ludwig et al., 2023; Mohr et al., 2023), demonstrating the urgency of climate adaptation measures. Most of these adaptation measures happen on the regional to local scale. Consequently, effective climate adaptation requires high-resolution and region-specific climate information capable of capturing fine-scale processes, such as deep convection triggering extreme precipitation (Masson-Delmotte et al., 2021; Pörtner et al., 2022). However, the spatial resolution of data available to date from GCMs or RCMs is still insufficient to resolve key local-scale processes, including deep convection, and therefore too coarse to fulfill the demand for adequate climate data to inform the development of local adaptation measures (Measham et al., 2011; Fünfgeld et al., 2023, 2026). Hence, additional downscaling to the convection-permitting scale is required (Schär et al., 2020).

Convection-permitting climate modeling refers to regional or global climate simulations conducted at kilometer-scale horizontal resolutions (typically 1–4 km), where deep convection is explicitly resolved rather than parameterized. This approach has been shown to substantially improve the representation of short-duration extreme precipitation, organized convective systems, and associated hydrological risks compared to coarser-resolution models (Prein et al., 2015; Kendon et al., 2020; Ban et al., 2021). In Europe, convection-permitting modeling has advanced through coordinated initiatives such as EURO-CORDEX and its Flagship Pilot Studies dedicated to very high resolution climate simulations (Giorgi and Gutowski, 2015; Coppola et al., 2020). Early breakthroughs in convection-permitting climate modeling (CPM) emerged from the WCRP CORDEX Flagship Pilot Study (FPS; Giorgi et al., 2009; Gutowski Jr. et al., 2016), which targeted high-resolution convective processes over Europe and the Mediterranean (Coppola et al., 2020), culminating in the first decade-long, multi-model convection-permitting ensemble for the Greater Alpine region (FPS-ALPS; Pichelli et al., 2021). Other recently produced convection-permitting climate ensembles are the UKCP Local ensemble (Kendon et al., 2020) covering the British Isles, or the KIT-KLIWA ensemble (Hundhausen et al., 2023, 2024) covering central and southern Germany including the Alps. Ex-

https://doi.org/10.5194/egusphere-2026-2517
Preprint. Discussion started: 11 June 2026

pected benefits of such CPM simulations are a better representation of the intensity distribution and diurnal cycle of precipitation (Fowler et al., 2021; Lucas-Picher et al., 2021; Hundhausen et al., 2024) due to the explicit treatment of convection, but also for 2 m temperature (Soares et al., 2024; Hundhausen et al., 2023), 10 m wind speed (Molina et al., 2024), and for application-relevant climate indices (Pinto et al., 2026). Nevertheless, the availability of such high-resolution kilometer-scale CPM simulations remains limited (Prein et al., 2015; Coppola et al., 2020; Ban et al., 2021; Lucas-Picher et al., 2021; Kendon et al., 2023).

One reason for the sparse availability of CPM simulations are the high computational costs, especially for large ensembles, even though the technical resources have significantly increased in recent years. Hence, most activities on the CPM scale only cover short time slices of 10 to 30 years or small domains of about 1000 km × 1000 km (Pichelli et al., 2021; Caldas-Alvarez et al., 2023). Pioneering work in global convection-permitting simulations is done, for example, by Stevens et al. (2019, 2020), but such global simulations are typically limited to a couple of months to a few years due to the prohibitive computational costs, and therefore, not suitable to derive statistics required for supporting climate change adaptation.

To overcome the high computational costs, one possibility is the application of statistical downscaling approaches. Under current climate conditions, such statistical models showed similar or even better results than dynamical downscaling models (e.g., Maraun et al., 2015; Gutiérrez et al., 2019). However, these models struggle to represent the unknown future climate conditions due to missing training data. Furthermore, the physical consistency between different variables (e.g., temperature and precipitation) is not ensured anymore, especially under strong climate change signals (Lanzante et al., 2018). Hybrid statistical-dynamical models aim to combine the benefits of both approaches, but are often limited to specific variables (Reyers et al., 2015). Other recently developed methods, such as so-called "RCM emulators" (Doury et al., 2023), are not yet suitable for operational use.

To address the lack of high-resolution climate data, the NUKLEUS ("Actionable local climate information for Germany") initiative (Sieck et al., 2026), as part of the funding program RegIKlim of the German Federal Ministry of Research, Technology, and Space (BMFTR), will deliver the first kilometer-scale convection-permitting multi-model climate ensemble for Germany. This ensemble will provide unprecedented spatial detail to evaluate past and future climate conditions and to support regional climate impact research as well as the creation of actionable knowledge for local climate adaptation initiatives in Germany. This study presents the characteristics of the simulations of the historical reference period (1961–1990) from the NUKLEUS ensemble and assesses their performance relative to reanalyses, and observation-based data sets. The evaluation is done for the basic meteorological variables (2 m temperature, precipitation, 10 m wind speed), and selected application-relevant climate indices.

A further requirement for the practical usability of climate data is its alignment with observations. For downstream applications in hydrology, agriculture, infrastructure planning, energy, and climate-risk assessments high-quality data sets that closely match observations are essential (Maraun and Widmann, 2018), which is usually achieved by performing a bias correction to the simulation output. In this context, bias correction denotes a statistical post-processing step that adjusts climate model output to reduce systematic deviations from observed climatology and distributional properties (e.g., mean, variability, and quantiles), thereby improving consistency with observational reference data for impact modeling. Here, we explore the benefits and lim-

https://doi.org/10.5194/egusphere-2026-2517
Preprint. Discussion started: 11 June 2026

itations of a standard and straightforward bias correction approach based on quantile delta mapping and analyze the resulting data sets in the context of downstream applicability.

This study is structured as follows: Sect. 2 describes the NUKLEUS climate ensemble, the used reference data sets, and the methods used for the evaluation and also the bias correction. In Sect. 3, the results of the evaluation of the basic meteorological variables (temperature, precipitation, and wind speed) are presented, and in Sect. 4, the performance regarding climate indices is evaluated. Section 5 compares the NUKLEUS ensemble to two existing regional climate model ensembles available for Central Europe. The effect of the bias correction on basic variables, climate indices, and possible consequences for downstream applications is given in Sect. 6. Finally, Sect. 7 discusses the results and lists the conclusions.

2 Data and methods

2.1 The NUKLEUS ensemble

NUKLEUS is a novel ensemble of high-resolution, convection-permitting climate simulations (CPM) for Germany at 3 km horizontal grid spacing (Sieck et al., 2026). Three CMIP6 global climate models (GCMs; see Sect. 2.1.1) were selected and each of them was dynamically downscaled by three regional climate models (RCMs, see Sect. 2.1.2). Hence, the NUKLEUS ensemble consists of 9 members. In a first step, each GCM was downscaled to an intermediate resolution of 0.11° (approximately 12 km) with each RCM covering the EURO-CORDEX domain (EUR-12, formerly named EUR-11) for the transient period 1950–2100. Second, the same RCMs were then used to further downscale the EUR-12 simulations to the high-resolution CPM simulations on the final resolution of 0.0275° (approximately 3 km) for a central European domain covering Germany and surrounding areas (CEU-3; cf. Fig. 1 in Sieck et al., 2026). Due to the higher computational costs, the CEU-3 simulations are only performed in time-slices of 30 years for the historical reference period 1961–1990 (Sect. 2.3) and the two global warming levels of +2 K and +3 K compared to preindustrial conditions (1881–1910, cf. Beier et al., 2026) using the ssp3-7.0 scenario (O'Neill et al., 2016).

In this study, we focus on the 3 km simulations of historical reference period 1961–1990, which is recommended by the World Meteorological Organization (WMO) and applied as the standard reference period for long-term climate change assessments by the DWD for Germany (World Meteorological Organization, 2017; Kaspar et al., 2021). For the 3 km future projections and climate change signals, we refer to Beier et al. (2026). The 12 km intermediate EUR-12 simulations of NUKLEUS have already been evaluated by Cusinato et al. (2026) with respect to the hydrological cycle, or Beier et al. (2026) in terms of the climate change signal of application-relevant climate indices, where the added value of the 3 km simulations compared to the 12 km simulations is also addressed.

2.1.1 GCM selection

The decision process of the GCM selection includes multiple aspects, closely following the CORDEX CMIP6 protocol (Gutowski Jr. et al., 2016; Katragkou et al., 2024). A basic requirement is the availability of the 3-dimensional forcing data for

https://doi.org/10.5194/egusphere-2026-2517
Preprint. Discussion started: 11 June 2026

the dynamical downscaling with a sufficient temporal resolution (minimum 6-hourly). A second criterion is a higher spatial resolution compared to CMIP5, which is supposed to improve the GCM results (Fernandez-Granja et al., 2021). In addition, the GCM simulations are desired to be as independent as possible from each other (Brunner et al., 2020), and should cover a plausible range of the equilibrium climate sensitivity (ECS) at double CO_2 (Nijsse et al., 2020). In a related effort, Sobolowski et al. (2023) compiled an extensive evaluation of the suitability of CMIP6 GCMs for a downscaling over Europe, selecting six GCMs in the so-called "EURO-CORDEX Balanced Ensemble Matrix" (BEM). Since the primary purpose of NUKLEUS is to provide reliable climate information for Germany, the representation of weather patterns in Central Europe is given the highest priority. To this end, the statistics of circulation weather types (CWTs; Jones et al., 1993) and the blocking index (Masato et al., 2013) are analyzed using preinstalled plugins on the Freva platform (Kadow et al., 2021) at the German Climate Computing Center (DKRZ), namely the CWT plugin (Schartner, 2016) and the 2D-blocking plugin (Richling, 2020). The CWTs are analyzed at a reference point in Central Europe at 50° N and 10° E. The blocking index calculation considers an area over the North Atlantic-European region between 75° W to 75°E and 30° N to 90° N, with enabled option of spatial filtering following Barriopedro et al. (2010).

The GCM performance for the above-mentioned aspects is evaluated using the ERA5 reanalysis (Hersbach et al., 2020; Bell et al., 2021) as benchmark. ERA5 is the latest generation of global reanalysis data provided by the European Center of Medium-range Weather Forecasts (ECMWF). It represents a detailed and realistic record of the global atmosphere, land and ocean surface at a horizontal resolution of 0.25° and a temporal resolution of 1 h for atmospheric variables, including 37 vertical pressure levels between 1000 hPa and 1 hPa. It covers the time period from 1940 up to present day.

Figure 1 shows the mean squared error (MSE) of the annual (seasonal) frequency of the CWTs and the blocking index for the six GCMs of the BEM against the ERA5 reanalysis based on daily values during the period 1980 to 2010. GCMs with smaller errors in all seasons (indicated by light colors) reproduce the typical distribution of weather patterns more accurately. The different period for the GCM selection is chosen, as ERA5 is expected to have a higher quality due to the assimilation of observations, including radiosoundings and satellite data (Bell et al., 2021).

Based on these criteria, the following three CMIP6 GCMs are selected for the NUKLEUS ensemble: EC-Earth3-Veg (hereafter ECE; EC-Earth Consortium (EC-Earth), 2019) with high (ECS > 4), MPI-ESM1-2-HR (hereafter MPI; Jungclaus et al., 2019; Schupfner et al., 2019) with medium, and MIROC6 (hereafter MIR; Tatebe and Watanabe, 2018; Shiogama et al., 2019) with low (ECS < 3) sensitivity. Consequently, the 12 km NUKLEUS simulations on the EUR-12 domain consist of a subset of the EURO-CORDEX CMIP6 ensemble for Europe, particularly for the BEM initiative (Sobolowski et al., 2023).

2.1.2 Regional climate models

For the downscaling, three regional climate models (RCMs) were chosen: ICON-CLM (hereafter ICON; Zaengl et al., 2015; Pham et al., 2021), COSMO-CLM (hereafter CCLM; Rockel et al., 2008; Baldauf et al., 2011), and REMO (Jacob and Podzun, 1997; Pietikäinen et al., 2025). While CCLM and REMO are well established (e.g., Sørland et al., 2021; Steger and Bucchignani, 2020; Pietikäinen et al., 2025), particularly for simulating the European climate, the climate version of ICON is new and applied and evaluated for the first time using other GCMs than global ICON simulations as forcing. However, the mod-

https://doi.org/10.5194/egusphere-2026-2517
Preprint. Discussion started: 11 June 2026

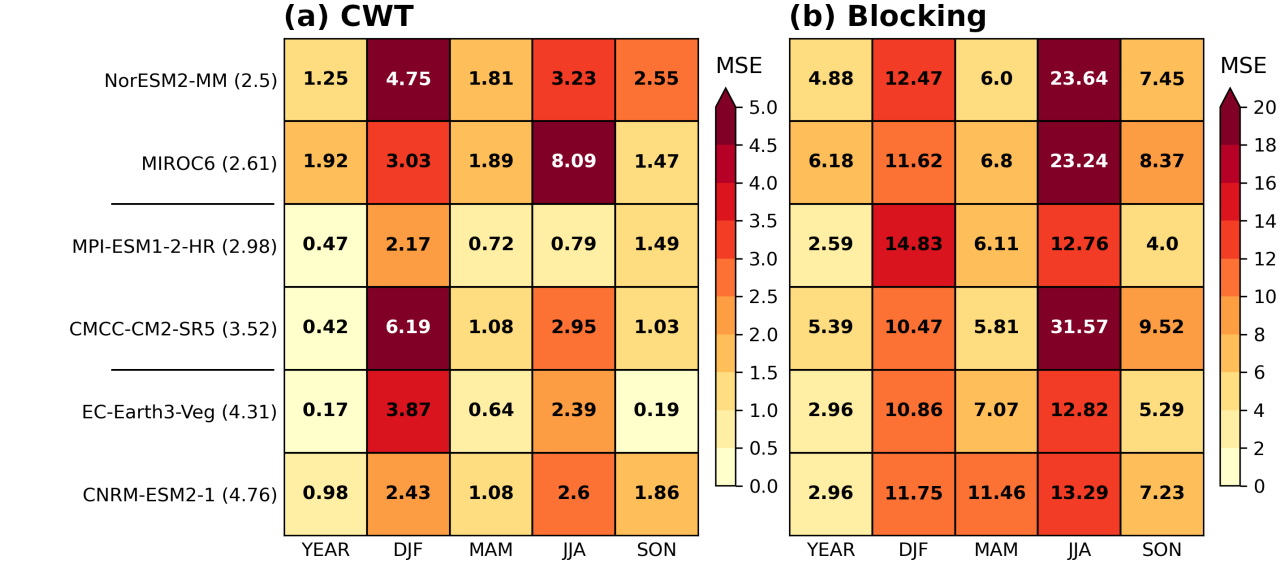

Figure 1. Representation of (a) circulation weather type (CWT) frequency over Central Europe, and (b) blocking index frequency over the North Atlantic-European region in CMIP6 simulations over Europe for each season and the whole year, depicted as mean squared error (MSE) against ERA5 reanalysis data during the period 1980 to 2010. The numbers in brackets behind the GCM name give the ECS in °C according to Smith et al. (2021), Table 7.SM.5, as part of Masson-Delmotte et al. (2021). The GCMs are sorted in ascending order by ECS from top to bottom, and the horizontal lines between the GCM names separate the three groups of low, medium, and high ECS.

eling groups contributing to the NUKLEUS ensemble were involved in the development and tuning of all three RCMs. We here provide only brief descriptions of each RCM, since comprehensive model descriptions and the corresponding specific configurations for the NUKLEUS ensemble are provided in detail by Sieck et al. (2026).

CCLM (version: CCLM-V6.0) is a non-hydrostatic model using a horizontal grid on curvilinear rotated geographical coordinates. In the vertical, it uses a terrain-following coordinate with 55 height levels up to a top height of 30 km above sea level (Sørland et al., 2021). For land surface processes, the multilayer soil model TERRA-ML is used (Grasselt et al., 2008). At the resolution of 3 km, deep convection is explicitly resolved, and only shallow convection is parameterized (Tiedtke, 1989).

ICON (version: ICON-CLM V2.6.5) is a non-hydrostatic model using an icosahedral grid with triangular shaped grid cells in the horizontal (Prill et al., 2023). The 3 km simulations use the R13B07 structure. During post-processing, the triangular grid is interpolated to the regular latitude-longitude grid CEU-3 which is also used for the other models. The vertical grid consists of 65 non-equidistant levels. ICON also uses TERRA-ML for land surface processes. The parameterization of shallow convection is basically the same as in CCLM but with the modifications implemented by Bechtold et al. (2008). Deep convection, again, is resolved explicitly.

REMO (version: REMO2020) is a hydrostatic model using a rotated latitude-longitude horizontal grid and 49 hybrid-sigma pressure levels in the vertical (Pietikäinen et al., 2025), with a non-hydrostatic extension called REMO-NH based on Göttel (2009) and Janjic et al. (2001). In the non-hydrostatic mode, which is used within NUKLEUS, only shallow convection is

https://doi.org/10.5194/egusphere-2026-2517
Preprint. Discussion started: 11 June 2026

parameterized. For surface processes, REMO uses a tile approach scheme depending on the fraction of land, water, or ice. The sea surface temperature (SST) is prescribed from the driving model, while for inland water bodies the module FLake (Mironov, 2008) is applied. All soil variables are initialized using ERA5 boundary conditions.

2.2 Reference data

The main observational data reference for this study is HYRAS-DE (version v5.0, hereafter referred to as HYRAS; Rauthe et al., 2013; Razafimaharo et al., 2020), which is used both for the general validation of the NUKLEUS simulations and for bias correction (see Sect. 2.4). This data set is provided by Germany's National Meteorological Service (Deutscher Wetterdienst; DWD). HYRAS contains gridded daily precipitation totals at a resolution of $1\,\mathrm{km} \times 1\,\mathrm{km}$, and also daily mean, maximum, and minimum temperatures at a $5\,\mathrm{km} \times 5\,\mathrm{km}$ resolution covering Germany. It is based on several thousand station measurements interpolated to a regular grid considering local characteristics such as elevation, exposition, and local climatology (Rauthe et al., 2013). HYRAS is available since 1951 and continuously updated up to present. It already served as reference in multiple previous studies on model evaluation and extreme event analysis (e.g., Ehmele et al., 2020; Ludwig et al., 2023).

As a complementary reference data set, the ERA5-Land reanalysis (Muñoz-Sabater et al., 2021) is used. The ERA5-Land reanalysis is driven by the coarser ERA5 (Hersbach et al., 2020; Bell et al., 2021) and provides hourly data of surface and soil variables for the land areas around the globe at a spatial resolution of 0.1° covering the period from 1950 to present. For the atmospheric part, it includes near-surface variables such as $2\,\mathrm{m}$ temperature, precipitation, and $10\,\mathrm{m}$ wind speed, where precipitation and wind are obtained from coarser ERA5 by simple linear interpolation between the two grids, while temperature estimates include a height correction (Muñoz Sabater et al., 2021). Expectedly, this locally leads to substantial differences between the NUKLEUS simulation output and ERA5-Land (see Sects. 3.3, 3.4, and 3.5). Therefore, a short quality assessment and classification of ERA5-Land using the same time period and observation-based reference data as Sieck et al. (2026) can be found in the supplemental material. Nevertheless, this study employs ERA5-Land as a reference data set for two primary purposes. First, it is used to evaluate the diurnal cycle of the NUKLEUS ensemble, as no other suitable hourly data with sufficient spatial representativeness is available for the 1961—1990 period. Second, it serves as the reference for evaluating the simulated wind data, since no other observation-based gridded wind data set is available for the entire period, even on a daily basis.

2.3 Basic analysis framework and statistical methods

To assess the performance of the NUKLEUS ensemble, we analyze the $2\,\mathrm{m}$ temperature, $10\,\mathrm{m}$ wind speed, and precipitation (hereafter referred to as the basic meteorological variables) in comparison with the reference data sets HYRAS and ERA5-Land. Both HYRAS and ERA5-Land are interpolated to the CEU-3 grid of the NUKLEUS simulations using remapping procedures of the cdo routines (Schulzweida, 2022) with a conservative remapping applied to precipitation sums and wind speed. Daily mean, maximum and minimum $2\,\mathrm{m}$ air temperature are interpolated using nearest neighbor remapping for HYRAS and bilinear remapping for ERA5-Land. Subsequently, a height correction considering the commonly used constant mean free-

https://doi.org/10.5194/egusphere-2026-2517
Preprint. Discussion started: 11 June 2026

atmosphere lapse rate of $0.0065\,\mathrm{K\,m^{-1}}$ (Dutra et al., 2020) was applied to the temperature data to account for topographic differences between the data sets.

All basic analyses are conducted on the native rotated curvilinear CEU-3 grid of the NUKLEUS simulations. The bias correction (Sect. 2.4) and climate indices calculation (Sect. 2.5.1) are performed on a regular latitude-longitude grid (CEU-3i) with slightly coarser horizontal grid spacing than the CEU-3 grid.

The basic meteorological variables are examined on various time scales ranging from years to hours (e.g., annual and diurnal cycles). The statistical representation of each variable is analyzed using probability density functions (pdfs) and quantified using the Perkins skill score (PSS; Perkins et al., 2007). For that, the data is clustered into equally distributed histogram classes with a bin width of $1\,\mathrm{K}$ for temperature, $0.5\,\mathrm{m\,s^{-1}}$ for wind, and $5\,\mathrm{mm}$ for precipitation. Additionally to the pdfs, the bias relative to the reference data is examined. For most analyses, the data of the entire year is considered, while for specific investigations, the data is clustered seasonally into spring (March to May, MAM), summer (June to August, JJA), autumn (September to November, SON), and winter (December to February, DJF).

The data is analyzed grid point-wise for entire Germany, and spatially aggregated over six pilot regions distributed across Germany (Fig. 2), which represent different topographic, climatic, and land use conditions, as well as socio-economic challenges for climate adaptation: the coastal region of East Frisia (EF) in northern Germany, the low mountain range area in the triangle of the federal states of Thuringia, Saxony, and Saxony-Anhalt (TSA), the county of Elbe-Elster (EE) in Eastern Germany characterized by strong agriculture and mining, the Pre-Alpine region (PAR) in southern Germany, and the two extended urban areas of Duisburg (DUI) and Stuttgart (STU). Within the main part of this study, the focus is put on the regions EF, TSA, and PAR. The results for the other pilot regions and entire Germany can be found in the supplemental material.

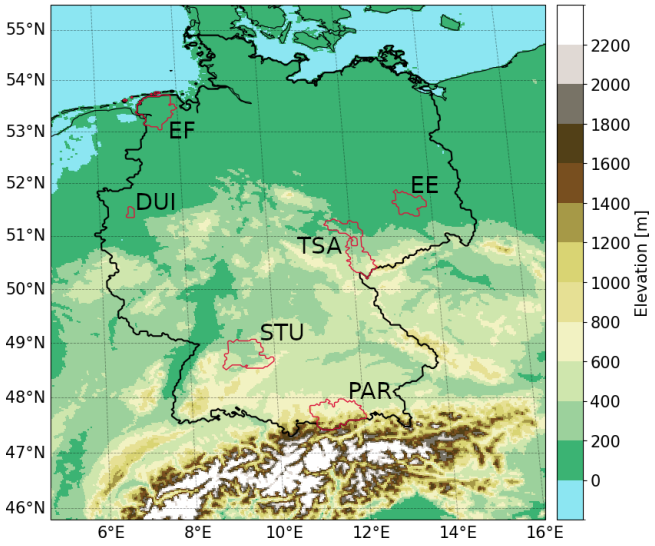

Figure 2. Topography of the study area on the $3\,\mathrm{km}$ central European grid (CEU-3) with the six selected pilot regions EF, DUI, STU, PAR, TSA, and EE (red contours) used for the statistical analysis. The black contour outlines Germany.

https://doi.org/10.5194/egusphere-2026-2517
Preprint. Discussion started: 11 June 2026

2.4 Bias correction

A bias correction is performed on daily precipitation totals and daily mean, minimum, and maximum 2 m temperature by applying the quantile delta mapping (QDM) approach described by Cannon et al. (2015). The core principle of the QDM is to adjust the cumulative distribution function (cdf) of model data so that it aligns with the observed cdf.

The bias correction is carried out by constructing the univariate empirical transfer function that maps simulated quantiles to the observed ones for the historical reference period. Univariate means that no correlations or dependencies between different variables are considered, and the variables are treated as independent. The daily HYRAS data (see Sect. 2.2) serve as observational reference. Prior to bias correction, model and observational data are remapped to the regular CEU3i grid (see section 2.3). The interpolation to CEU-3i is done conservatively for precipitation. For mean, minimum, and maximum 2 m temperature nearest neighbor interpolation without height correction for the simulated data sets is used. Precipitation fields are filtered by applying a threshold of 0.05 mm to handle small numerical values as zero known as the drizzle effect (Berg et al., 2012). To account for seasonal variability, monthly differentiated empirical transfer functions are derived. Spatial biases are corrected by constructing empirical transfer function of each grid point individually. Following the recommendation of Cannon et al. (2015), the number of quantiles used for the empirical transfer functions was determined by the length of the data to be corrected, which here corresponds to the number of time steps in the 30-year historical reference period. No further subsampling of the data was applied (Hyndman and Fan, 1996). Consequently, the QDM incorporates the complete distribution of values. For precipitation, this includes accounting for the frequency of dry days.

Strictly speaking, the method applied within this manuscript is a pure quantile mapping using the transfer function described above. The full quantile delta mapping considering the climate change signal via a delta modification (Cannon et al., 2015; Ivanov et al., 2018) is applied by Beier et al. (2026) to the future projections of NUKLEUS corresponding to global warming levels of +2 K and +3 K.

2.5 Derived indices

One of the main aims of NUKLEUS is the provision of user-relevant and actionable climate information. Thus, we here derive various climate indices in order to provide a more practical and application-relevant description of the simulated climate than the basic meteorological variables. The used indices are derived from uncorrected and bias-corrected model data, and the reference data.

2.5.1 Extreme climate indices

We here use the extreme climate index definitions based on daily 2 m temperature and precipitation that were defined by the Joint CCl/CLIVAR/JCOMM Expert Team on Climate Change Detection and Indices (ETCCDI[1]) and its extension ETSCI by WMO and WCRP (Karl et al., 1999; Climpact, 2024).

[1] http://www.clivar.org/organization/etccdi/etccdi.php, last access: 29 January 2026

https://doi.org/10.5194/egusphere-2026-2517
Preprint. Discussion started: 11 June 2026

In this study, a subset of five ETCCDI climate indices is chosen, and the respective definitions are provided in Table 1. Heat and cold stress are analyzed using the annual number of summer days (SU), the percentage of hot days per year with a maximum temperature above the climatological 90th percentile (TX90p), and the annual number of frost days (FD). Precipitation extremes are investigated using the contribution of very wet days (annual percentage of precipitation above the climatological 95th percentile) to the annual wet-day precipitation (R95ptot) and the annual number of very heavy rain days, defined as a daily precipitation sum of at least 20 mm (R20mm). These indices can be categorized into two groups: the first group is based on fixed universally applied numerical thresholds (SU, FD, R20mm), while the second group uses relative percentile based thresholds, which depend on the grid point-specific distribution (Tx90p, R95ptot).

Climate indices for both the CPM simulations and reference data sets are calculated using the ClimDexCalc2 toolbox based on the package ClimPACT (Alexander and Herold, 2016; Climpact, 2024). The toolbox interpolates the basic meteorological variables to the CEU-3i grid (see Sect. 2.3) prior to index calculation. The interpolation to CEU-3i is done conservatively for precipitation and bilinear for mean, minimum, and maximum 2 m temperature without height correction.

2.5.2 Precipitation severity index

In order to provide an event-based analysis of the impact of the bias correction on daily precipitation, the precipitation severity index (PSI) developed by Caldas-Alvarez et al. (2023) is applied, which provides a spatially and temporally aggregated measure, in contrast to the purely grid-point based ETCCDI indices described in the previous section. The PSI quantifies the severity of precipitation events based on the intensity at each grid-point with respect to a given climatological threshold, as well as the spatial extent and the temporal persistence of the precipitation event. In this study, the PSI is calculated using a persistence of three days and the climatological 95th percentile as threshold, in order to detect the most extreme precipitation events. Precipitation events with highest intensities, largest extent, and longest persistence exhibit the highest PSI. Due to the

Table 1. Overview of the selected ETCCDI climate indices, with daily maximum temperature TX_{ij} and daily minimum temperature TN_{ij} of day i in year j. TX_{in} is the corresponding 90th percentile within the period 1961–1990. RR_{wj} is the daily precipitation amount of wet days w (daily precipitation sum ≥ 1 mm) in year j. W is the total number of wet days in j, and RR_{ij} is the daily precipitation amount on day i in year j. $RR_{wn}95$ is the corresponding 95th percentile on wet days within the period 1961–1990.

Climate index	Abbreviation	Unit	Calculation
Summer days	SU	days	$TX_{ij} > 25\,^{\circ}C$
Hot days	TX90p	%	$TX_{ij} > TX_{in}90$
Frost days	FD	days	$TN_{ij} < 0\,^{\circ}C$
Very heavy rain days	R20mm	days	$RR_{ij} \geq 20$ mm
Contribution from very wet days	R95ptot	%	$\frac{\sum_{w=1}^{W} RR_{wj}}{\sum_{i=1}^{I} RR_{ij}}$, where $RR_{wj} > RR_{wn}95$

https://doi.org/10.5194/egusphere-2026-2517
Preprint. Discussion started: 11 June 2026

consideration of extent and persistence, the PSI is suitable to assess the impact of the bias correction on the spatial and temporal coherence of precipitation signals.

3 Analysis of basic meteorological variables

3.1 Annual and seasonal mean biases

To assess the performance of the NUKLEUS ensemble on climatological time scales, the spatial distribution (two-dimensional maps) and aggregated spatial mean values of the annual and seasonal mean bias of temperature and precipitation are analyzed. The overview of the seasonal mean biases of all basic meteorological variables spatially averaged over Germany and all NUKLEUS pilot regions can be found in Figs. S10–S13.

Regarding the daily mean temperature, all models exhibit a meridional gradient in the annual mean bias against HYRAS, with predominantly warm (cold) biases in southern (northern) Germany (Fig. 3; the annual mean temperature in HYRAS is shown in Fig. S4a). Despite the height correction applied to HYRAS, orographic-related bias patterns remain visible across all simulations after interpolation to the model grid. The ensemble mean bias averaged over entire Germany (provided as the mean bias $\pm$ one standard deviation as an estimate of the ensemble bandwidth; Fig. S10) is very low during spring (0.07 ± 0.43 K) and fall (0.05 ± 0.39 K). For summer (0.57 ± 0.61 K) and winter (0.38 ± 0.92 K), moderate warm ensemble mean biases are found for entire Germany.

All MIR-driven simulations exhibit the coldest annual mean biases, while ECE- and MPI-driven simulations exhibit comparable magnitudes of the biases (Fig. 3). For each driving GCM, the spatial structures of these biases are very similar in the CCLM and ICON simulations, though the ICON simulations generally show slightly lower values. The REMO simulations predominantly exhibit warm biases throughout Germany, especially when driven by ECE and MPI.

Temperature biases vary in both sign and magnitude across seasons, exhibiting distinct patterns that can be attributed either to the driving GCM or to the RCM (Fig. S10). The MIR-driven simulations display particularly strong seasonal biases, with a cold bias in DJF and a warm bias in JJA. This pattern is consistent across Germany and within each pilot region, leading to the moderate annual mean bias noted previously (Fig. 3). By contrast, MPI-driven simulations exhibit a persistent warm bias in DJF across all pilot regions, without any offsetting cold bias, resulting in the largest warm biases in the annual mean (Fig. 3). Except for JJA, ICON simulations generally exhibit the strongest cold bias. In JJA, however, the coldest biases occur in CCLM simulations and the warmest in REMO simulations, a pattern that is consistent across all driving GCMs and pilot regions.

Daily temperature extremes generally show a consistent behavior: daily maximum temperature exhibits colder biases than daily mean temperature during most seasons and for most regions (cf. Figs. S12 and S10). In contrast, daily minimum temperatures exhibit very similar biases as daily mean temperature with a tendency to warmer biases (cf. Figs. S13 and S10). This pattern suggests a systematic underestimation of temperature extremes, with smaller daytime maxima in the RCM simulations compared to HYRAS. When driven by MIR or MPI, both CCLM and ICON consistently exhibit a cold bias in the annual mean daily maximum temperature (Fig. S7; the annual mean daily maximum temperature in HYRAS is shown in Fig. S4b). In contrast, the REMO simulations generally show a warm bias in the annual mean of daily maximum temperature. This bias is

https://doi.org/10.5194/egusphere-2026-2517
Preprint. Discussion started: 11 June 2026

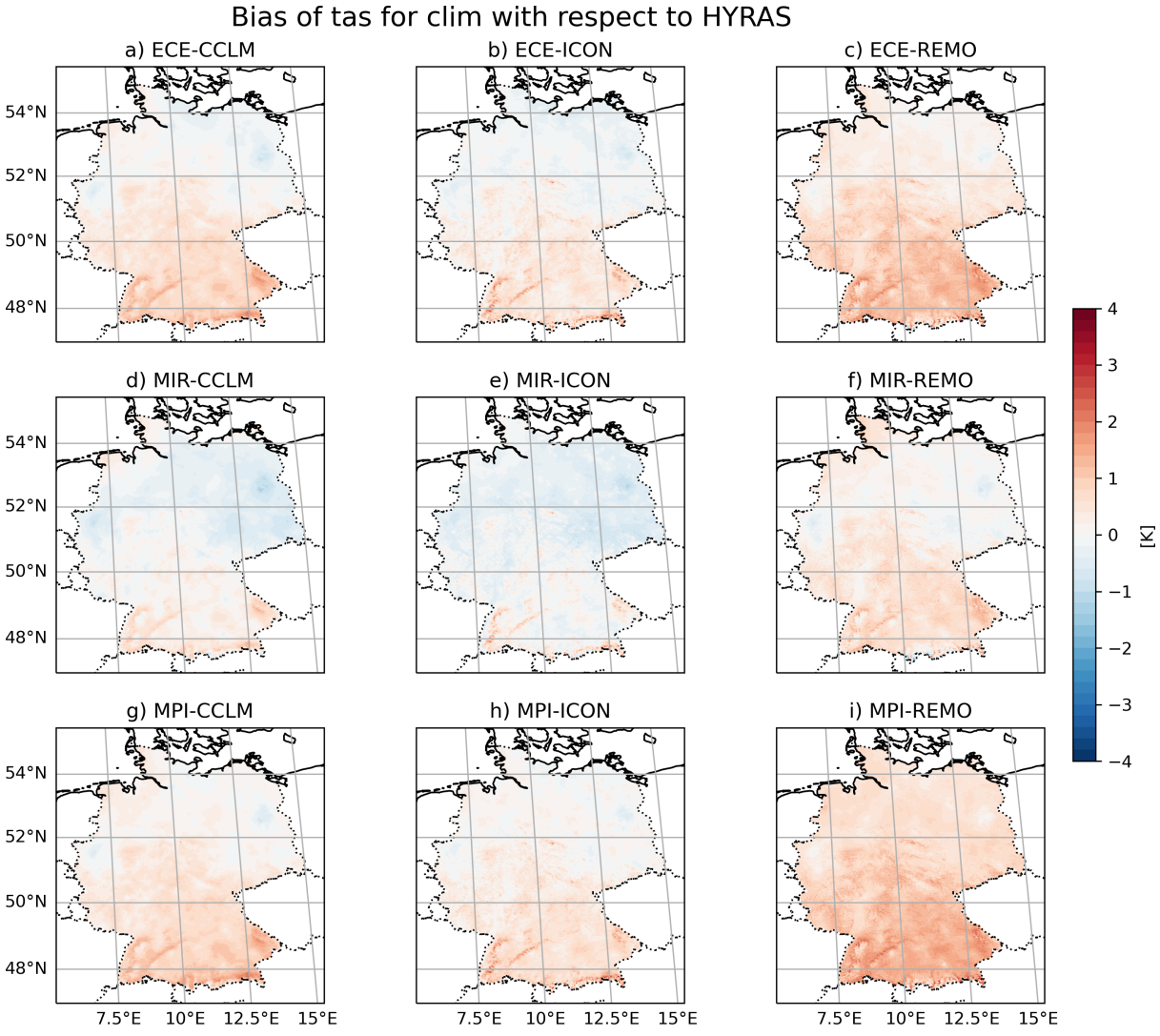

Figure 3. Annual mean bias of daily mean 2 m temperature (tas) of the ECE- (a–c), MIR- (d–f), and MPI-driven (g–i) RCM simulations with CCLM (a,d,g), ICON (b,e,h), and REMO (c,f,i) with respect to HYRAS. The absolute values of HYRAS are shown in Fig. S4a.

strongly influenced by the land surface scheme, resulting in pronounced warm biases over urban areas and marked cold biases over lakes.

The annual mean relative biases of precipitation also exhibit clear orographic patterns, with strong wet biases and modest dry biases (Fig. 4; the annual mean daily precipitation sum in HYRAS is shown in Fig. S4d). Overall, the simulations predominantly exhibit wet biases with the largest ensemble mean biases during winter and the smallest ensemble-mean biases during summer (Fig. S11). Spatially averaged over entire Germany the ensemble mean bias is 20.14 ± 5.25 mm per month during winter and 4.21 ± 7.23 mm per month during summer.

https://doi.org/10.5194/egusphere-2026-2517
Preprint. Discussion started: 11 June 2026

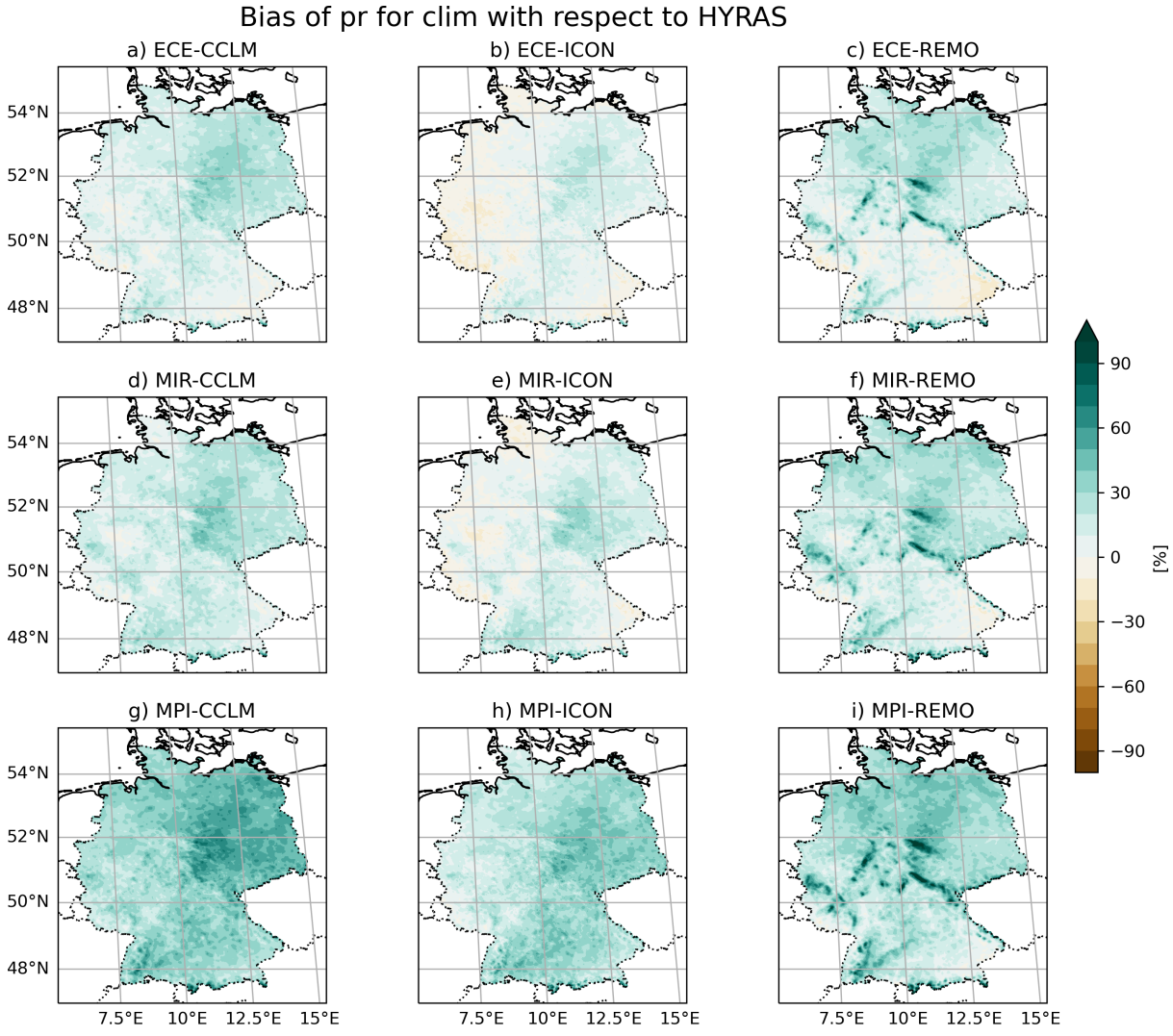

Figure 4. Relative annual mean bias of monthly precipitation totals (pr) of the ECE- (a–c), MIR- (d–f), and MPI-driven (g–i) RCM simulations with CCLM (a,d,g), ICON (b,e,h), and REMO (c,f,i) with respect to HYRAS. The absolute values of HYRAS are shown in Fig. S4d.

Spatial gradients of the precipitation biases are less pronounced than those for temperature. The bias in ICON and CCLM simulations exhibits a weak zonal gradient, which is of opposite sign in northern and central Germany compared to the south. In relative terms, the strongest wet biases are found in central and eastern Germany, where low absolute values prevail (Fig. S4d), as well as in the Alpine region near Germany's southern border, where annual mean precipitation is high (Fig. S4d). Locally, the REMO simulations exhibit very strong wet biases that are also linked to orography. These biases likely result from the unsmoothed topography applied in REMO, which can enhance uplift processes.

https://doi.org/10.5194/egusphere-2026-2517
Preprint. Discussion started: 11 June 2026

Dry biases occur in only a few regions and seasons across the simulations. The ECE-driven simulations constitute the primary exception to this pattern (Fig. S11). The largest dry biases are found for JJA. Similar to the biases found for temperature, the ICON simulations show the strongest (dry) biases in autumn, winter and spring. However, there is no obvious relationship between temperature and precipitation biases on seasonal timescales (Figs. S10 and S11).

The spatial gradients and orographic patterns found in the annual mean temperature and precipitation biases are also evident from the reanalysis-driven evaluation simulations presented in Sieck et al. (2026). This suggests that these are features arising from the CPM simulations independent of the imposed GCM-specific boundary conditions. As expected, the biases in the GCM-driven simulations analyzed here are larger than those in the evaluation simulations of Sieck et al. (2026), but they remain of the same order of magnitude.

Overall, all members of the NUKLEUS ensemble are considered to provide reasonable representations of the mean climate state during the historical reference period with moderate biases in near-surface air temperature and precipitation. Nevertheless, for some of the applied models and regions non-negligible climatological biases are found especially on seasonal time scales. Thus, for downstream applications that require an accurate consideration of absolute values, a bias correction of the provided data set is recommended. A discussion of the detected biases with respect to previous regional climate model ensembles is provided in Sect. 5. Furthermore, the biases are discussed in Sect. 7 with respect to the simulated interannual variability (see Sect. 3.2).

3.2 Interannual and interseasonal variability

The RCM simulations reproduce the observed temperature variability reasonably well, as indicated by the box plots in Fig. 5. To enable a direct comparison of variability across models and reference data sets, we subtracted the median of each model, period, and region from the corresponding data set (corresponding figures without subtraction of the median are presented in the supplemental material in Figs. S16 and S17). In the annual mean, the interquartile range (IQR) of the individual simulations exhibits a width comparable to the IQR obtained from HYRAS (Figs. 5a and S14a). For PAR and TSA the simulated variability covers a wider range compared to HYRAS, with considerably higher deviations from the median towards low annual mean temperatures.

For DJF (Fig. 5b), the simulations exhibit a homogeneous IQR for PAR and TSA similar to the IQR obtained from HYRAS. For the EF region, MPI- and MIR-driven simulations exhibit smaller IQR compared to HYRAS. Similar to HYRAS, many of the simulations contain strong negative outliers and, thus, seem to reproduce the occurrence of single anomalously cold seasons. Conversely, during JJA (Fig. 5c) the REMO simulations display strong positive outliers that substantially exceed the variability observed in HYRAS. These deviations are most pronounced in the MPI-REMO simulation. This is also true for entire Germany and the other pilot regions (Fig. S14c). In combination with the previously discussed warm biases in all REMO simulations during JJA (Fig. S10), these strong positive outliers, suggests that individual years may experience particularly high temperature deviations relative to HYRAS. Separately, the RCM simulations show moderate over- and underestimation of the IQR during JJA, with no clear pattern linked to the specific RCMs or driving GCMs.

https://doi.org/10.5194/egusphere-2026-2517
Preprint. Discussion started: 11 June 2026

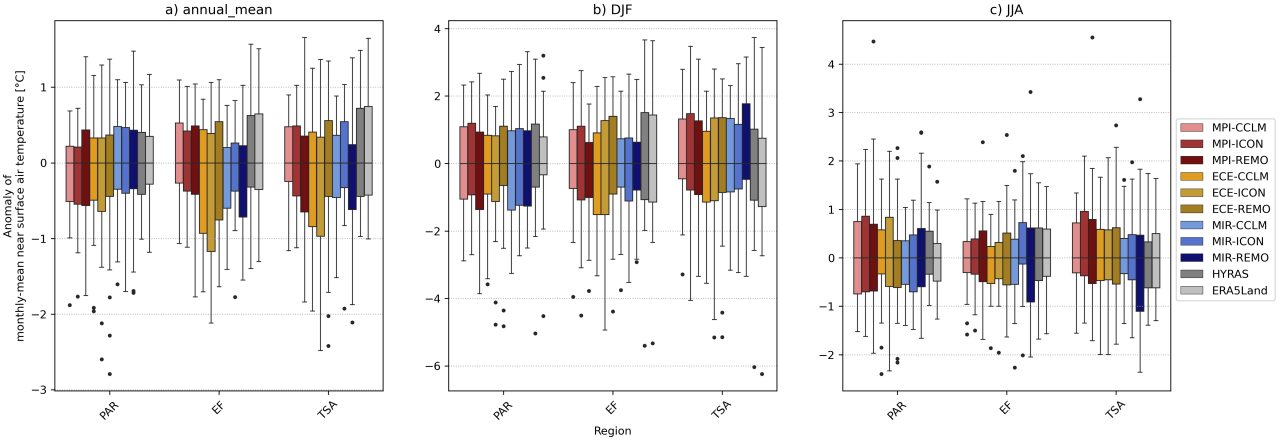

Figure 5. Box plots of median-adjusted annual and seasonal mean 2 m temperature simulated by the RCMs and HYRAS for the pilot regions PAR, EF and TSA, representing the interannual (a) and the interseasonal variability for DJF (b) and JJA (c). To focus on the variability, the median of each model, period, and region was subtracted from the respective data. The center line indicates the median. The box edges represent the interquartile range (IQR). The whiskers mark the farthest point from the nearest box edge within 1.5 × IQR. The dots mark outliers. Note the different scales of the vertical axes.

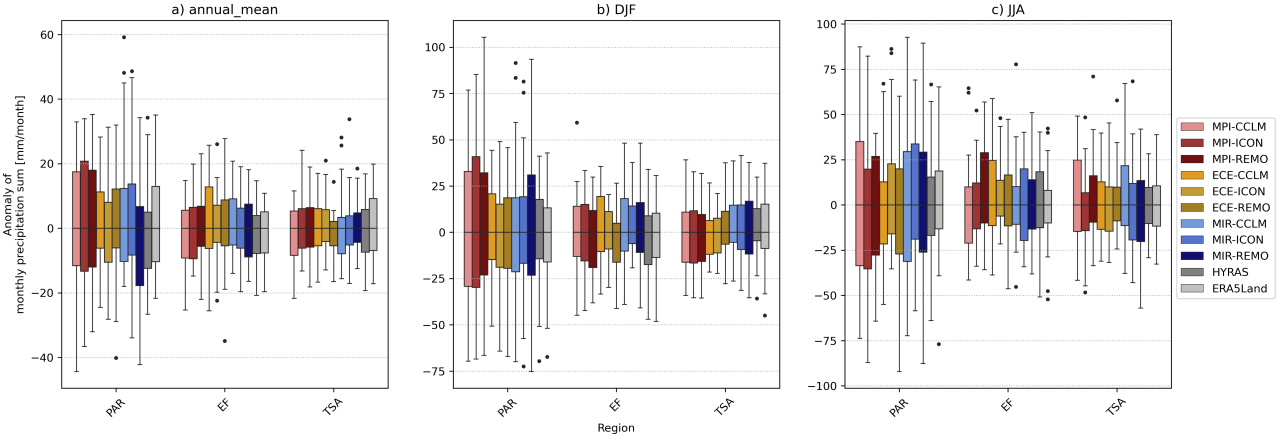

Figure 6. Same as Fig. 5, but for annual and monthly mean (within a season) precipitation totals.

Regarding precipitation, the RCMs successfully capture the regional pattern of the interannual and interseasonal variability present in HYRAS. This is evidenced by the fact that the simulated variability scales proportionally with that of HYRAS across different regions, especially during JJA (Figs. 6 and S15; corresponding figures without subtraction of the median are presented in the supplemental material in Figs. S18 and S19). However, the regional differences in precipitation variability are more pronounced in the simulations than in HYRAS. This is particularly evident in the PAR and STU regions, which show high simulated variability in MPI- and MIR-driven simulations across all periods (annual mean, DJF, and JJA). Especially during DJF, there are considerably higher positive deviations from the median compared to HYRAS for single regions (PAR, STU).

https://doi.org/10.5194/egusphere-2026-2517
Preprint. Discussion started: 11 June 2026

The contrast between summer and winter precipitation is more pronounced in the simulations than in HYRAS for the PAR and TSA regions, whereas it is well represented for EF. The annual mean variability for entire Germany is represented very well (Fig. S15a).

3.3 Annual cycles

The annual cycles of monthly mean 2 m temperature and the respective monthly biases towards HYRAS for the selected pilot regions are shown in Fig. 7. The course of the annual cycles is well captured by the models and for all regions. However, most models show a positive bias throughout the year. The MPI- and ECE-driven simulations, for instance, show the highest positive deviations to HYRAS with up to 2 K in the winter and spring months (namely December to April), which are more pronounced in PAR than in EF and TSA. In summer, the MPI- and ECE-driven simulations show mainly smaller negative biases of up to –1 K in EF and TSA, while PAR shows again positive biases up to 1 K. In contrast, the MIR-driven simulations show the highest biases in summer (EF: May–September, TSA and PAR: June–August) and negative differences in winter (EF and TSA about –2 K in December and PAR –1 K in January). With a few exceptions, where the differences are below 1 K (e.g., a few MIR-driven simulations in PAR, the MPI-driven simulations in all three regions, the ECE-driven simulations in EF and TSA), all RCMs driven by the same GCM behave in the similar way. ERA5-Land shows negative deviations to HYRAS throughout the year in PAR, with the greatest difference in winter (December: –2.5 K) and decreasing towards August. For all other regions, ERA5-Land is similar to HYRAS.

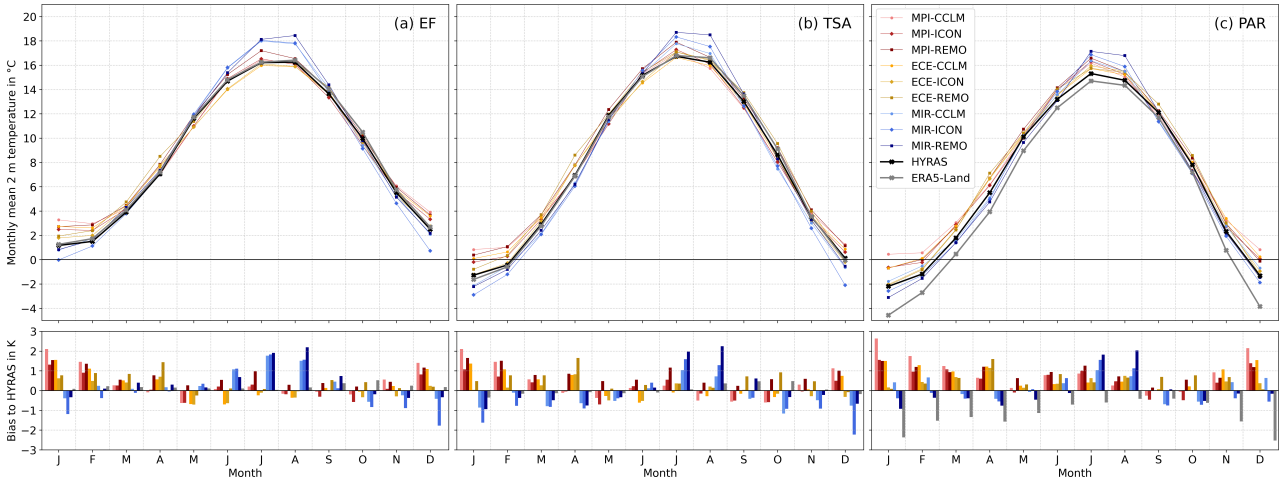

Figure 7. Annual cycle of monthly mean 2 m temperature for the pilot region of (a) EF, (b) TSA, and (c) PAR for HYRAS (black, crosses), ERA5-Land (gray, crosses), and the NUKLEUS ensemble: reddish colors mark the CPM simulations driven by MPI, yellowish colors those driven by ECE, and blueish those driven by MIR; dots indicate the CCLM simulations, diamonds the ICON simulations, and squares the REMO simulations. The bar plot at the bottom gives the bias towards HYRAS of all simulations and ERA5-Land.

https://doi.org/10.5194/egusphere-2026-2517
Preprint. Discussion started: 11 June 2026

The annual cycles of temperature in STU, EE, and DUI show similar characteristics (Fig. S20). Again, the MIR-driven simulations show positive biases in summer and negative biases in winter with similar magnitudes. In STU and EE, the MPI- and ECE-driven simulations also show similar signs and magnitudes as for the areas presented above. Only for DUI, these simulations show lower biases throughout the entire year within the range of ± 1 K.

In general, the presented results demonstrate that the driving GCM dominates the bias signal for temperature in all regions. This is partly in line with the findings by Sieck et al. (2026), who, likewise, found a similar bias signal in the reanalysis-driven simulations of all RCMs, for example, in EF or DUI. However, they found an RCM dependency in other regions with contrasting bias signals (e.g., positive bias of REMO and negative bias of CCLM and ICON in TSA). Furthermore, the biases found by Sieck et al. (2026) are of contrasting sign compared to the results presented in this study in most regions, although the magnitude is comparable.

The annual cycles of monthly precipitation sums is shown in Fig. 8. The course of the HYRAS annual cycle is well captured by all models in all regions. The highest absolute values and the strongest variations within the annual cycle is found in the mountainous PAR region, with a distinct summer peak, while it is more homogeneous throughout the year in the coastal EF region with a small minimum in early spring. The simulations show the lowest differences to HYRAS (below 20 %) in summer for EF (June and July), TSA (August), and PAR (June–August), and the greatest differences in autumn and winter (up to 80 % in December, PAR, MPI-CCLM). The rather small biases in summer further tend to be negative, while the rest of the year mainly positive biases are found. However, it should be noted that HYRAS is not undercatch corrected regarding measurement errors primarily caused by technical or physical factors at the measurement site, which leads to an underestimation of the actual precipitation amounts.

For STU, EE, and DUI, likewise wet biases are found throughout almost the entire year, except a few models during summer (Fig. S21). The magnitude of the wet biases is the smallest in DUI. The EE region shows similar magnitude as TSA, which

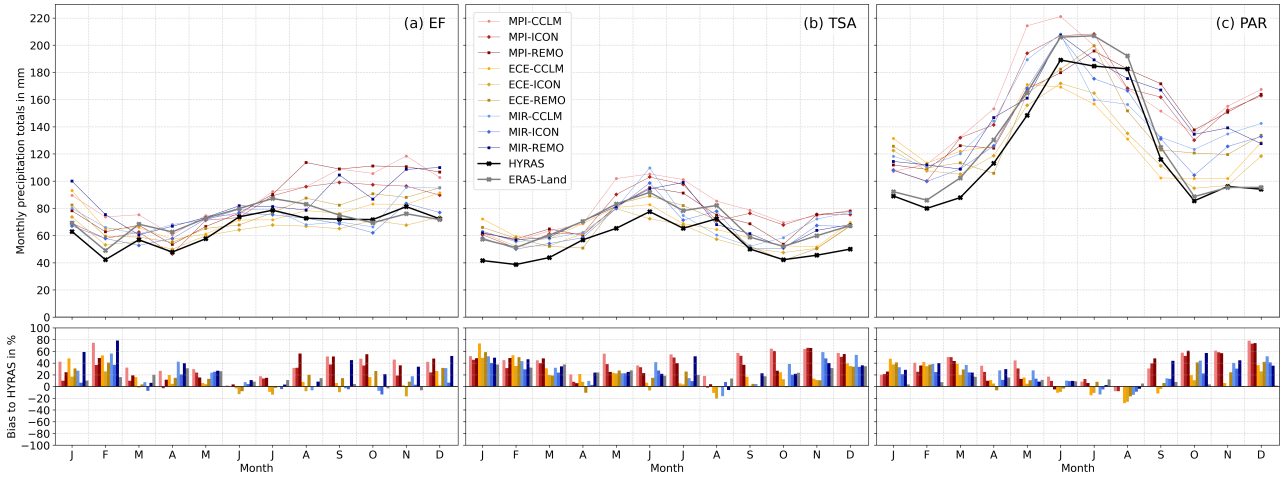

Figure 8. Same as Fig. 7, but for monthly precipitation totals.

https://doi.org/10.5194/egusphere-2026-2517
Preprint. Discussion started: 11 June 2026

could be related to the spatial proximity of the two regions to each other. The relative biases in STU in the individual months show similarities to PAR, although the absolute monthly sums are lower in STU than in PAR. As for EF, the rather flat region of DUI shows a rather flat annual cycle with a small minimum in early spring, while there is a distinct summer peak in the STU region, which is characterized by a more complex orography. This means that the orographic signal especially in summer precipitation is well captured by the simulations.

A consistent dependency to the driving GCM is found for precipitation, as the MPI-driven simulations tend to have the strongest positive biases, while the ECE-driven simulations tend to have the lowest biases in all regions (Figs. 8 and S21). Compared to the ERA5-Land reanalysis, HYRAS shows mostly lower monthly precipitation. The presented results are in line with the general evaluation by Sieck et al. (2026) with mainly positive precipitation biases in all regions for all models. Negative biases mainly occur during summer and autumn. However, the magnitude of the biases presented here is expectedly larger than in Sieck et al. (2026).

Annual cycles of monthly mean 10 m wind speeds are shown in Fig. 9, with higher wind speeds towards the northern and more coastal regions. For TSA and PAR, all simulations show higher wind speeds than ERA5-Land (up to 2 $\mathrm{m\,s^{-1}}$), whereas for EF, the overestimation is either less than 1 $\mathrm{m\,s^{-1}}$, or negative (up to –0.7 $\mathrm{m\,s^{-1}}$) for MIR-REMO. However, a rough quality assessment of ERA5-Land (see supplemental material) reveals a general underestimation of ERA5-Land compared to observation-based data set of the same order of magnitude as for the NUKLEUS ensemble. Taking this into account, the NUKLEUS ensemble performs well. Furthermore, the larger deviations for regions with more complex terrain likely originate from the coarse native resolution of ERA5-Land, which strongly smooths orographic details relevant for accurate near-surface wind representation.

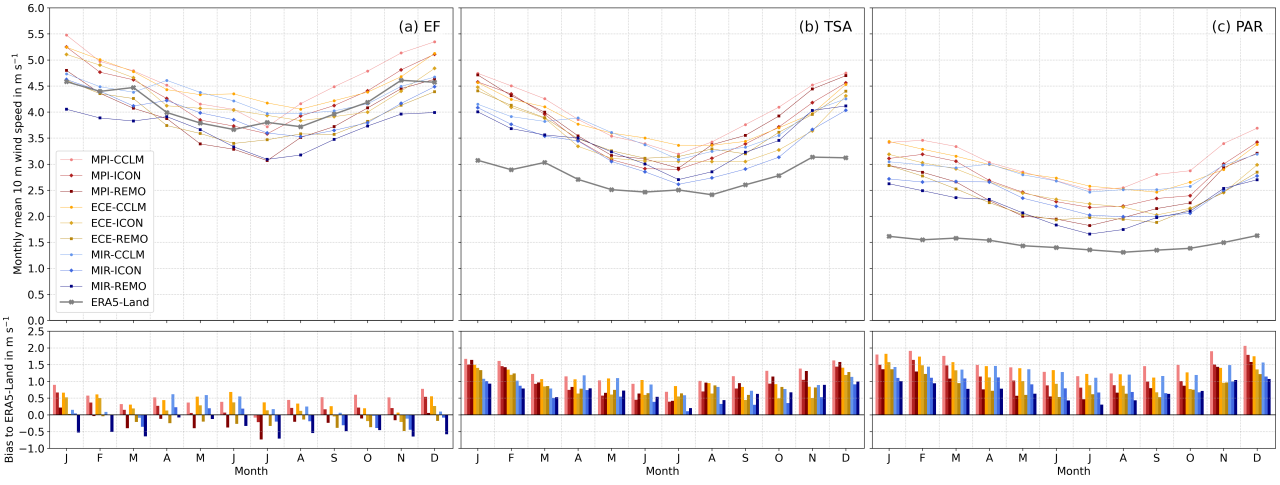

Figure 9. Same as Fig. 7, but for monthly mean 10 m wind speed. Note that there is no wind data in HYRAS, and, therefore, the bias is calculated towards ERA5-Land.

https://doi.org/10.5194/egusphere-2026-2517
Preprint. Discussion started: 11 June 2026

The qualitative findings for the annual cycles of the mean wind speed for STU, EE, and DUI are similar (Fig. S22). The lowest deviation towards ERA5-Land is found for DUI, which also exhibits rather flat terrain, while the deviations in EE and STU are higher and of comparable magnitude as for TSA and PAR, respectively. All models show positive deviations compared to ERA5-Land in all months for EE and STU, while for DUI a few simulations, but mostly MIR-REMO, exhibit slightly negative deviations.

3.4 Frequency distributions

We explore the statistical representation of the basic meteorological variables on daily time scales by probability density functions (pdfs). For the daily mean 2 m temperature (Figs. 10 and S23), the pdfs of all simulations and reference data sets form a double maximum for all pilot regions, with the highest frequencies around 0 to 5 °C (winter maximum) and around 10 to 15 °C (summer maximum). The three MIR-driven simulations (shown in blueish tones in Fig. 10) are positioned at the extremes of the temperature distribution in most pilot regions. This placement indicates that these simulations produce both cold and warm extremes more frequently than the other data sets. Furthermore, the summer maximum of the MIR-driven simulations in the EF and TSA region is slightly shifted towards warmer values. The distributions of the NUKLEUS ensemble are within the spanned range of both HYRAS and ERA5-Land, except for ERA5-Land in PAR, which might be a result of its coarser original resolution together with the mountainous orography in that area.

The annual mean wet biases presented in Sect. 3.1 are also evident in higher frequencies of remarkable daily precipitation totals (above 20 mm) in almost all models and regions compared to HYRAS and also ERA5-Land (Figs. 11 and S24). Over the entire range of values, the pdfs of all models in all pilot regions are above those of HYRAS or ERA5-Land with increasing

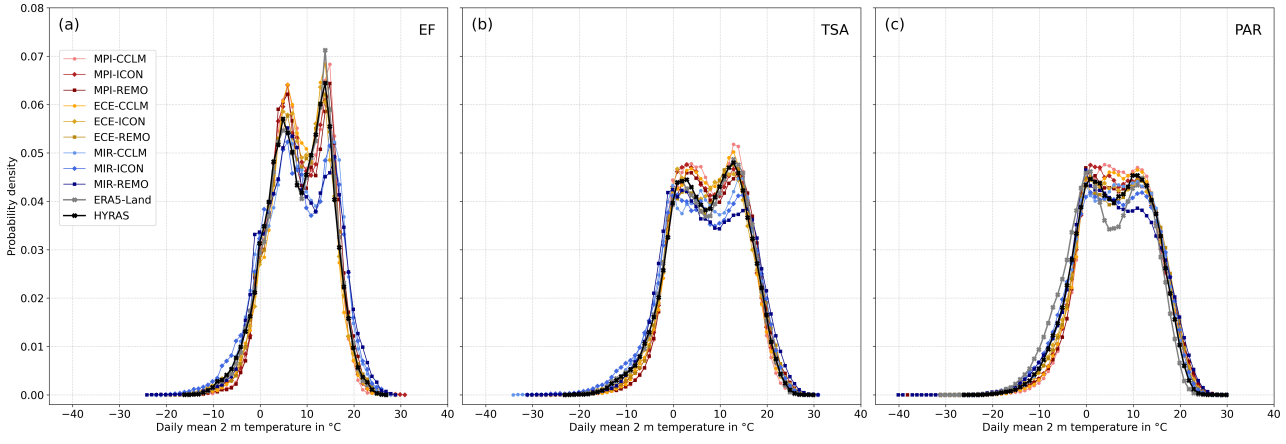

Figure 10. Frequency distribution of daily mean 2 m temperature (bin width 1 °C), taking into account every single grid point within the pilot region of (a) EF, (b) TSA, and (c) PAR for HYRAS (black, crosses), ERA5-Land (gray, crosses), and the NUKLEUS ensemble: reddish colors mark the CPM simulations driven by MPI, yellowish colors those driven by ECE, and blueish those driven by MIR; dots indicate the CCLM simulations, diamonds the ICON simulations, and squares the REMO simulations.

https://doi.org/10.5194/egusphere-2026-2517
Preprint. Discussion started: 11 June 2026

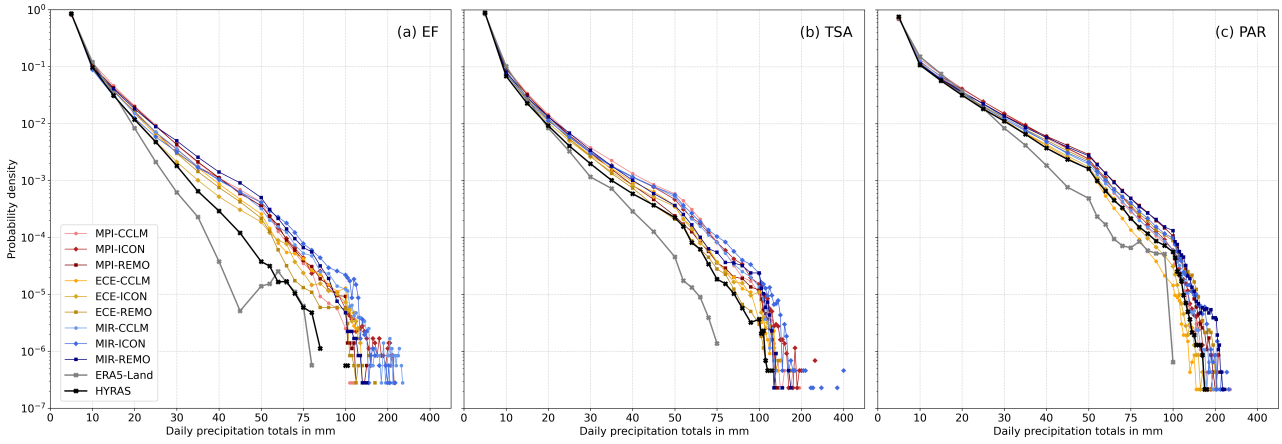

Figure 11. Same as Fig. 10, but for daily precipitation totals (bin width 5 mm). Please note the non-linear x-axis.

distance towards the extremes, except for ECE-CCLM and ECE-ICON in PAR. This strongly agrees with the results of the reanalysis-driven simulations in Sieck et al. (2026). In general, the MIR-driven simulations exhibit the highest frequencies of remarkable daily precipitation (above 20 mm), while the ECE-driven simulations exhibit the lowest frequencies. Furthermore, there are daily precipitation amounts in the simulations far beyond the maximum values of HYRAS. The maximum simulated daily precipitation amount within the investigation areas is found in TSA in the MIR-ICON simulation with around 400 mm, which is already above the maximum observed 24 h precipitation amount for Germany of 353 mm (Deutscher Wetterdienst, 2003). One reason for the higher precipitation could be that CPMs explicitly capture each simulated convective cell in total, whereas in HYRAS, convective cells are only captured when passing one of ground-based observation station, on which HYRAS is based on. Same applies for ERA5-Land, which is likewise based on measurements for the reference period, but additionally its coarser native resolution is not convection-permitting, and therefore not capable in resolving convective cells in detail.

The distributions of simulated daily mean 10 m wind speed (Figs. 12 and S25) show large variability and a clear dependency on the used RCM. The pdfs of the REMO simulations consistently differ from those of the CCLM or ICON simulations across all regions. This deviation manifests as either a shift of the maximum probability towards slightly lower wind speeds (approximately –0.5 m s−1 in PAR and DUI) or as a broader main body of the distribution in all other pilot regions. For PAR (Fig. 12c) and STU (Fig. S25c), the CCLM simulations are also grouped together, with a small shift (around 0.5 $\mathrm{m\,s^{-1}}$) towards higher wind speeds. The absolute maximum wind speed in the individual pilot regions, however, cannot be assigned to a specific group of RCMs or GCMs.

The wind speed of the NUKLEUS ensemble is evaluated against ERA5-Land, as no other suitable high-resolution observational data set exists for the historical period. Consequently, the results are strongly influenced by the region and its properties, particularly the orography. This explains the strong agreement between NUKLEUS and ERA5-Land in flat regions like the coastal EF (Fig. 12a) and the relatively flat DUI (Fig. S25a). More complex orography manifests in larger differences between

https://doi.org/10.5194/egusphere-2026-2517
Preprint. Discussion started: 11 June 2026

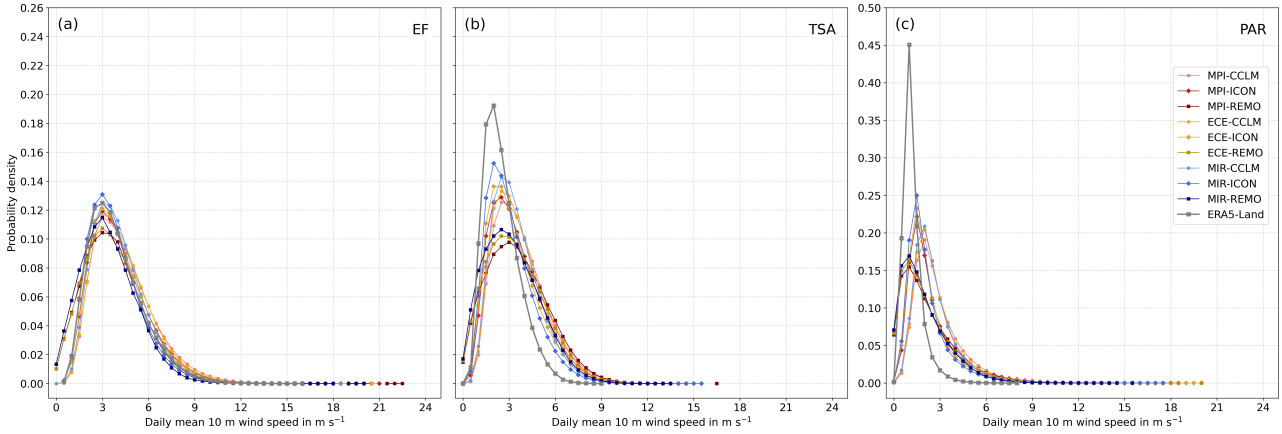

Figure 12. Same as Fig. 10, but for daily mean 10 m wind speed (bin width 0.5 $\mathrm{m\,s^{-1}}$). Note that there is no wind data in HYRAS.

ERA5-Land and NUKLEUS in terms of the shape of the pdfs or the maximum wind speed. However, the location of the maximum probability agrees well between NUKLEUS and ERA5-Land in all pilot regions except for the mountainous PAR region. The maximum wind speeds are higher in NUKLEUS than in ERA5-Land, which might also be a result of the coarser native resolution of ERA5-Land and, therefore, a different representation of the land surface and its interaction with the atmosphere. Furthermore, a general underestimation of ERA5-Land compared to observation-based data was detected (see supplemental material).

We further quantify the differences of the above pdfs against HYRAS (temp and prec) and ERA5-Land (wind) by calculating the Perkins skill score (PSS; Tables 2 and S1). For temperature, the NUKLEUS ensemble generally performs well. Most simulations achieve a PSS above 0.90 in all pilot regions, except for the three MIR-driven simulations in the coastal EF region. The ECE-driven simulations mostly show PSS values even above 0.95.

For precipitation, the ensemble demonstrates even higher skill, with nearly all simulations achieving PSS values above 0.95 across all regions. The primary exceptions are the MPI-CCLM simulations in four of the six pilot regions and the MIP-ICON simulation in PAR. Consistently, the ECE-driven simulations show the highest skill, with most values exceeding 0.98. The skill of the historical simulations is higher than for the ERA5-driven evaluation runs of Sieck et al. (2026). One possible explanation for this could be the longer time series (30 years historical versus 10 years evaluation), thereby reducing the statistical uncertainty arising from rare extreme events.

For the daily mean wind speed, the PSS shows mixed results, with the highest values (mostly above 0.90) in the rather flat EF and DUI regions, and the lowest (below 0.60) in the mountainous PAR region. The PSS in the TSA, EE, and STU region, that are characterized by shallow mountain ranges, is mainly between 0.70 and 0.90. As discussed above, the low PSS for wind is expected to originate from the coarse native resolution of ERA5-Land and the general underestimation compared to observation-based data sets due to the pure interpolation from the coarser ERA5 grid (see Sect. 2.2 and the supplemental material).

https://doi.org/10.5194/egusphere-2026-2517
Preprint. Discussion started: 11 June 2026

Table 2. Perkins skill score (PSS) using HYRAS as reference data set for daily mean 2 m temperature and daily precipitation totals, and ERA5-Land as reference for daily mean 10 m wind speed in the pilot regions EF, TSA, and PAR for all members of the NUKLEUS ensemble. PSS ≥ 0.95 are marked in **bold**, $0.90 \leq$ PSS < 0.95 are marked in *italics*. Note that due to rounding to two decimal places, the same rounded PSS can be marked with both types.

Model	2 m temperature			Precipitation			10 m wind speed		
	EF	TSA	PAR	EF	TSA	PAR	EF	TSA	PAR
MPI-CCLM	*0.93*	*0.94*	*0.94*	*0.95*	*0.95*	*0.93*	*0.90*	0.68	0.40
MPI-ICON	*0.94*	**0.96**	**0.95**	**0.97**	**0.96**	*0.95*	**0.95**	0.76	0.56
MPI-REMO	*0.92*	*0.94*	*0.95*	**0.96**	**0.96**	**0.96**	*0.92*	0.67	0.58
ECE-CCLM	*0.93*	**0.96**	**0.96**	**0.98**	**0.97**	**0.98**	*0.91*	0.71	0.42
ECE-ICON	**0.96**	**0.97**	**0.97**	**0.99**	**0.99**	**0.99**	**0.96**	0.80	0.57
ECE-REMO	**0.96**	**0.97**	**0.96**	**0.98**	**0.98**	**0.98**	*0.92*	0.70	0.60
MIR-CCLM	0.90	*0.95*	**0.98**	**0.98**	**0.97**	**0.96**	*0.95*	0.74	0.43
MIR-ICON	0.90	*0.93*	**0.96**	**0.99**	**0.98**	**0.98**	**0.97**	0.85	0.60
MIR-REMO	0.89	*0.92*	*0.94*	**0.97**	**0.97**	**0.97**	0.89	0.73	0.62

3.5 Diurnal cycles

The diurnal cycles of 2 m temperature (Fig. 13) show an almost synchronous course between ERA5-Land and the simulations in all regions. The daily maximum is reached at hours 13–14, while the daily minimum is reached at hours four to five. In all REMO simulations and pilot regions, the daily maximum and minimum temperature occurs 1 h later than in ERA5-Land. Interestingly, Sieck et al. (2026) found an opposite shift of REMO in all regions when only June and July were taken into account. The lowest diurnal range (minimum to maximum) is found in the EF region, while the highest is found in PAR. The simulated range of 2 m temperature agrees well with ERA5-Land except for the mountainous PAR region, where ERA5-Land exhibits considerably lower values. Hence, the deviations of the NUKLEUS simulations are the highest in PAR with up to 4 K, and comparatively low in EF with mostly ± 0.5 K). This is largely consistent with the ERA5-Land quality assessment presented in the supplemental material, which indicates a good agreement of ERA5-Land with observations in EF or Germany in general, but substantial negative deviations in PAR of up to 2 K, particularly during the night. Taking this into account, the NUKLEUS data would still show a clear warm, albeit smaller, bias in PAR during nighttimes. The different magnitudes of the deviations are likely a result of the coarse native resolution of ERA5-Land, which has the highest impact in mountainous regions. However, the REMO simulations show deviations of up to 1 K, especially in the afternoon, which is mainly due to the general temporal shift.

The diurnal temperature cycles for STU, EE, and DUI exhibit similar characteristics (Fig. S26). For DUI and STU, the NUKLEUS ensemble shows higher temperatures than ERA5-Land throughout the entire day, while for EE the ERA5-Land

https://doi.org/10.5194/egusphere-2026-2517
Preprint. Discussion started: 11 June 2026

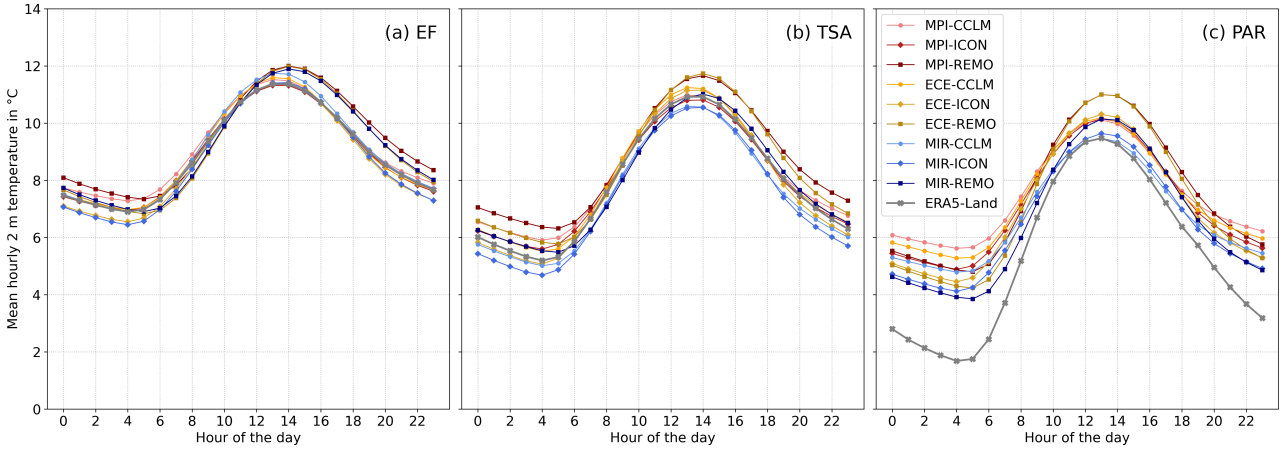

Figure 13. Diurnal cycle of mean hourly 2 m temperature for the pilot region of (a) EF, (b) TSA, and (c) PAR for ERA5-Land (gray, crosses), and the NUKLEUS ensemble: reddish colors mark the CPM simulations driven by MPI, yellowish colors those driven by ECE, and blueish those driven by MIR; dots indicate the CCLM simulations, diamonds the ICON simulations, and squares the REMO simulations.

data is within in the spanned range of the simulations. The temporal shift of the daily maximum is only visible in EE for MPI-REMO and ECE-REMO. However, the 1 h shift of the daily minimum is likewise present in all regions. With respect to the evaluation by Sieck et al. (2026), the magnitude of the deviations against ERA5-Land is comparable in most regions (all models within ±1.5 K), except for PAR (up to 4 K).

The simulated diurnal cycles of precipitation (Fig. 14) show a higher variability among the individual NUKLEUS simulations and exhibit remarkable differences to ERA5-Land. In EF and TSA, the diurnal cycles are more homogeneous throughout the day with a small maximum in the afternoon, which is up to 3 h later in the simulations than in ERA5-Land. The diurnal cycle in the mountainous PAR region is more pronounced with a clear maximum in the afternoon, which occurs up to 2 h later in the simulations than in the reanalysis. Due to this shift, an underestimation of the simulations in EF and TSA at noon and an overestimation in PAR in the afternoon and evening is found. However, Dai (2024) compared ERA5 diurnal cycles with observations on a global scale and found a shift of about 2 h to earlier hours for precipitation. Since ERA5-Land precipitation is simply interpolated from ERA5 data (see Sect. 2.2), it can be assumed that this shift is also present in ERA5-Land. Hence, the NUKLEUS simulations are likely more in phase with reality than the presented results suggest. While the amplitudes of ERA5-Land and the models are almost the same in EF and TSA, all REMO simulations show higher amplitudes than ERA5-Land in PAR. The diurnal precipitation cycles of the DUI, EE, and STU region (Fig. S27) show similar characteristics as for EF and TSA.

Regarding the diurnal cycles of 10 m wind speed (Fig. 15), the differences between simulations and ERA5-Land show a similar pattern as found for the annual cycles (see Fig. 9). In TSA and PAR, wind speeds in ERA5-Land are about 1–2 $\mathrm{m\,s^{-1}}$ lower than in the NUKLEUS simulations, with higher deviations during the day than at night. In EF, the NUKLEUS simulations span a range of $\pm 0.5\,\mathrm{m\,s^{-1}}$ around ERA5-Land for most of the day. Only in the early afternoon, when the maximum wind

https://doi.org/10.5194/egusphere-2026-2517
Preprint. Discussion started: 11 June 2026

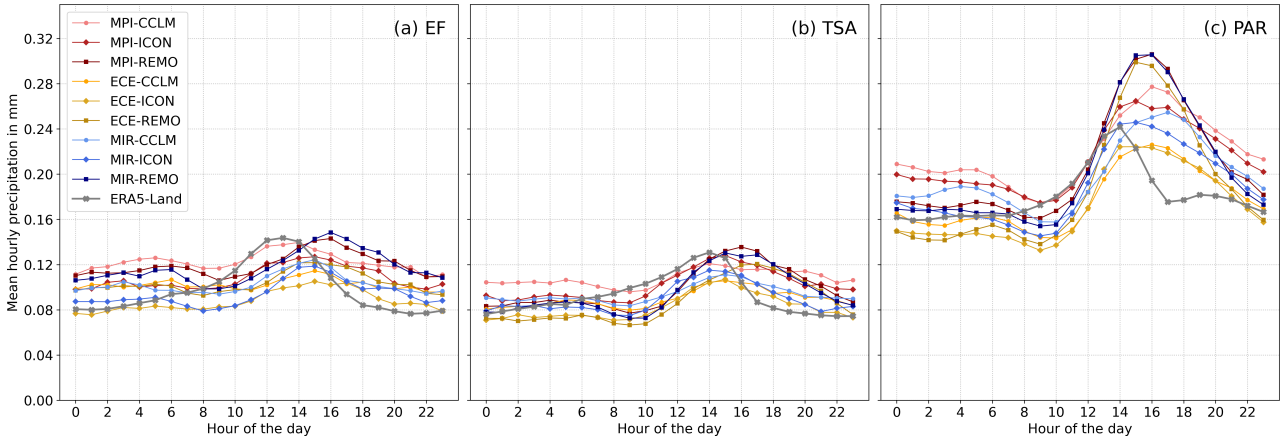

Figure 14. Same as Fig. 13, but for the mean hourly precipitation.

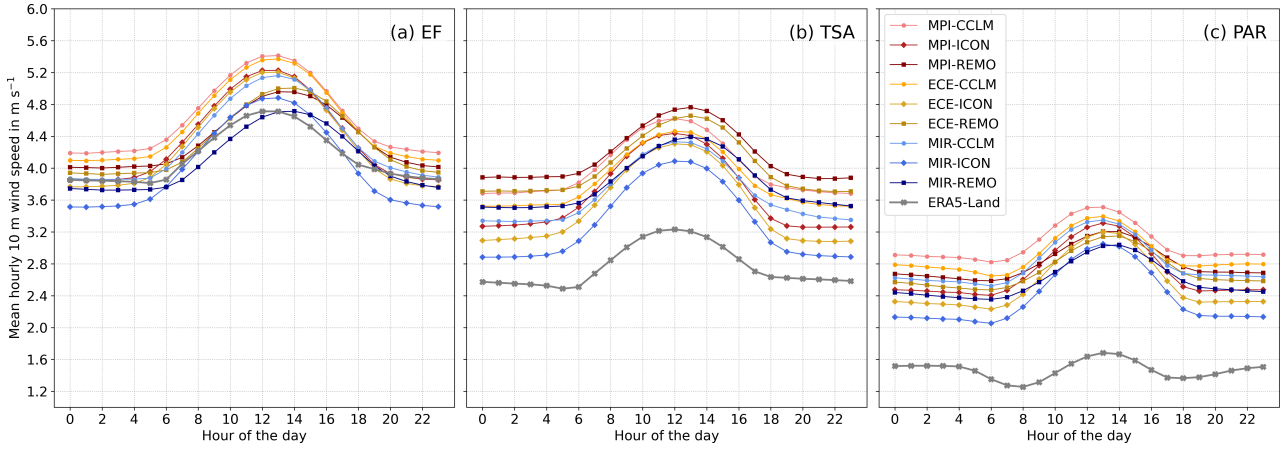

Figure 15. Same as Fig. 13, but for the mean hourly 10 m wind speed.

speeds occur, almost all NUKLEUS simulations show higher wind speeds than ERA5-Land. However, from Fig. S2 it is evident, that ERA5-Land underestimates wind speeds compared to observations of up to $2\,\mathrm{m\,s^{-1}}$ in PAR throughout the entire day, and up to $0.7\,\mathrm{m\,s^{-1}}$ for EF in the early afternoon. Taking this into account, the NUKLEUS ensemble is within the range of uncertainty of the reference data. Furthermore, the analyses reveal a temporal shift of 1 h towards the afternoon for all REMO simulations and in all regions compared to ERA5-Land, which is in line with Sieck et al. (2026), who found similar pattern in REMO considering the summer months June and July, only. In PAR, ERA5-Land exhibits a decline of the wind speed in the morning, which is slightly present in some simulations. Furthermore, ERA5-Land shows an increase of wind speed from the afternoon towards the evening, while the simulations show nearly constant values during this time of the day. As previously mentioned, the large deviations between simulations and ERA5-Land in TSA and PAR, might result from the coarse resolution

https://doi.org/10.5194/egusphere-2026-2517
Preprint. Discussion started: 11 June 2026

of ERA5-Land, which is not capable to cover local wind systems such as the mountain–valley circulation, while the finer 3 km NUKLEUS simulations might capture these phenomena including convection better.

For the DUI, EE, and STU regions (Fig. S28), the diurnal wind cycles show a similar pattern as in the focus regions. The REMO simulations likewise show a delay of about 1 h. Furthermore, in EE, REMO simulations show higher wind speeds than the other simulations. In contrast, the ICON simulations are grouped at the lower edge of the range of values in STU. In all regions, the NUKLEUS ensemble exhibits higher wind speeds than ERA5-Land, with the smallest differences in the rather flat DUI area.

4 Analysis of climate indices

4.1 Temperature-based indices

The annual number of summer days (SU; Figs. 16a for the focus areas and Fig. S29a for the other pilot regions and entire Germany) varies regionally, with lower counts in coastal and mountainous areas (EF, PAR) and higher counts in inland and low-mountain regions (TSA, EE, DUI, STU). The range spanned by the entire NUKLEUS ensemble encompasses the value ranges of both HYRAS and ERA5-Land, but both the median and variability of individual ensemble members differ substantially from HYRAS. SU depends on the RCM used, with CCLM simulations yielding the lowest SU per pilot region and REMO the highest. Similar dependencies were found by Sieck et al. (2026). Regarding the driving GCMs, MPI-driven simulations generally have lower SU than MIR- and ECE-driven simulations, though this signal visually seems less distinct than for the RCM dependency. However, MIR-driven simulations tend to have the highest SU, which is in line with the general warm bias found in Sect. 3.1 for these simulations.

The distributions of the annual hot days TX90p (Figs. 16b and S29b) reveal similar median values among all NUKLEUS ensemble members, HYRAS, and ERA5-Land, and also the spanned range of values is comparable among all data sets. This means that within the space of an individual member or data set, the proportion of TX90p values above the climatological 90th percentile and the interannual variability of TX90p are comparable, however, this does not imply that the 90th percentiles themselves are of similar magnitude. A slightly larger interannual variability can be found for the MPI-REMO simulations in PAR, DUI, and STU, and the ECE-REMO simulation in EF.

For the annual number of frost days (FD; Figs. 16c and S29c), a similar pattern as for SU can be detected. First, FD varies across regions with the lowest values in DUI and EF, and the highest numbers in PAR. The DUI region is characterized by a high amount of urbanization, which affects the general temperature level, while in the coastal EF region, the impact of the North Sea, acting as a heat reservoir is noticeable. The higher altitudes in the PAR region are generally characterized by lower temperatures, which explains the higher FD. In comparison with HYRAS and ERA5-Land, the NUKLEUS ensemble as a whole is capable to cover the observed range of values, even though individual members reveal a distinct bias. The majority of simulations underestimate the median FD over the 30-year period in most regions. The second pattern regarding FD is the dependency on the RCM. CCLM tends to simulate higher FD, while REMO tends to be the lowest. This is in line with the results in Sieck et al. (2026). In contrast to SU, a more pronounced relation to the used GCM can be found for FD, as the

https://doi.org/10.5194/egusphere-2026-2517
Preprint. Discussion started: 11 June 2026

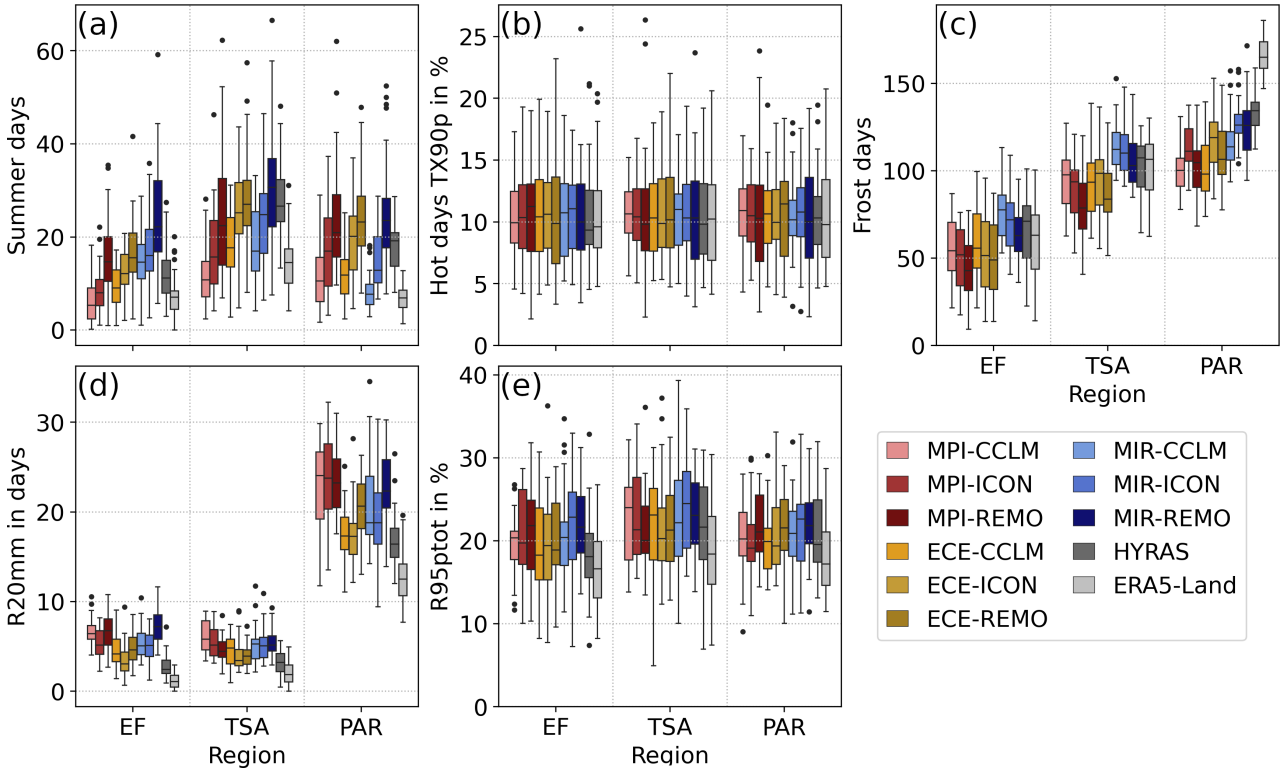

Figure 16. Box plots of the selected climate indices of the annual number of (a) summer days, (b) hot days with temperatures above the 90th percentile (TX90p), (c) frost days, (d) very heavy rain days with daily totals above 20 mm (R20mm), and (e) the contribution of very wet days with daily totals above the 95th percentile to the total annual precipitation (R95ptot) for the pilot regions EF, TSA, and PAR for the period 1961–1990 for HYRAS (dark gray), ERA5-Land (light gray), and the NUKLEUS ensemble: reddish colors mark the CPM simulations driven by MPI, yellowish colors those driven by ECE, and blueish those driven by MIR. The center line indicates the median, the box edges the interquartile range (IQR), and the whiskers extend to 1.5 × IQR. The dots mark outliers.

MIR-driven simulations show a positive offset compared to the ECE- or MPI-driven simulations. Thus, the identified overall cold bias of the MIR-driven simulations in Sects. 3.1 and 3.4 is also reflected in increased FD.

4.2 Precipitation-based indices

Intensive precipitation is analyzed using the annual number of days with precipitation totals exceeding 20 mm (R20mm; Figs. 16d and S29d). All NUKLEUS simulations display a consistent wet bias relative to HYRAS across all regions and even more for ERA5-Land, which exhibits lower R20mm than HYRAS. This is in line with the results presented in the previous sections and also with Sieck et al. (2026) for the ERA5-driven simulations. This is likely due to the already mentioned different representation of convection and native resolution. The NUKLEUS simulations can be grouped by the driving GCM, with MPI-driven simulations showing the highest R20mm and ECE-driven simulations the lowest. Overall, differences among pilot

https://doi.org/10.5194/egusphere-2026-2517
Preprint. Discussion started: 11 June 2026

regions are modest, with simulations typically spanning 0 to 15 days per year. In PAR, R20mm is considerably higher, with values exceeding 30 days per year, likely due to orographically enhanced precipitation in its mountainous terrain.

The contribution of very wet days with daily totals above the 95th percentile to the total annual precipitation (R95ptot; Figs. 16e and S29e) shows less variability among the individual models and a smaller difference to HYRAS compared to R20mm. This is in line with Sect. 3.1, showing a more or less spatially homogeneous relative bias, and due to the percentile-based definition of R95ptot versus the threshold-based definition of R20mm. Median values of R95ptot are largely in the range of 20 and 25 %. The interannual variability of all models and HYRAS likewise covers a similar range in all regions, with approximately 10 to 35 %. Only two simulations (MPI-CCLM and MIR-ICON) exceed an R95ptot of over 40 % in EE. Hence, the NUKLEUS ensemble is capable of simulating the observed range of values. Nevertheless, the median of the individual members tend to be slightly higher than HYRAS in most regions, except the EE region, where 6 out of 9 NUKLEUS simulations have a lower median than HYRAS. For all pilot region, the values in ERA5-Land are considerably lower than in the other data sets. As R95ptot also focuses on the heavy tail of the precipitation distribution, the limited representation of convection in the two reference data sets might explain the differences. There are no evident relations to the driving GCM or the used RCM.

With respect to the evaluation in Sieck et al. (2026), the presented results, such as higher medians in the simulations and similar ranges, strongly align. On the other hand, the current results also provide evidence of the importance of bias correction as post-processing in order to make the CPM data usable, particularly for fixed threshold variables like SU, R20mm, and FD (cf. Pinto et al., 2026).

5 Comparing NUKLEUS to existing RCM ensembles

To place the NUKLEUS ensemble within the context of other regional climate model ensembles available for Central Europe, we compare it to two already existing ensembles (partially) covering Germany: the KIT-KLIWA ensemble (Hundhausen et al., 2023, 2024; Pinto et al., 2026) and EURO-CORDEX (Jacob et al., 2014).

5.1 KIT-KLIWA

The KIT-KLIWA ensemble consists of four GCMs downscaled with CCLM to 2.8 km horizontal resolution, covering central and southern Germany including the Alps (cf. Hundhausen et al. (2023) for near-surface air temperature, and Hundhausen et al. (2024) for precipitation). The used CMIP5 GCMs include EC-Earth and MPI-ESM-LR. This provides the possibility to compare simulations of similar GCM-CPM combinations between the NUKLEUS ensemble and KIT-KLIWA, though in different model versions. Pinto et al. (2026) provided an analysis of basic meteorological variables and extreme climate indices in KIT-KLIWA against HYRAS for the reference period 1991–2020. In the following, we always refer to Pinto et al. (2026) in order to compare NUKLEUS against KIT-KLIWA over the central and southern part of Germany, that is covered by both ensembles.

https://doi.org/10.5194/egusphere-2026-2517
Preprint. Discussion started: 11 June 2026

The annual mean temperature biases in KIT-KLIWA for single models are of similar magnitude as in NUKLEUS, and also exhibit similar imprints of orography. The biases of the MPI-driven CCLM simulations in both ensembles are comparable. In ECE-driven CCLM simulations, a cold bias was found in KIT-KLIWA, while there is a warm bias in NUKLEUS. These minor differences may arise from the differences in the applied model versions (both GCM and RCM) as well as the different investigation periods. Furthermore, there are two interesting aspects to mention: first, HadGEM2-ES in KIT-KLIWA exhibits a strong warm bias. In NUKLEUS, there is no such outstanding bias related to one single GCM. Yet, the biases in ECE-REMO and MPI-REMO are only slightly smaller. Second, none of the simulations in NUKLEUS exhibits a cold bias for entire southern Germany, as the KIT-KLIWA member CNRM-CM5 does, which also exhibits substantial precipitation biases (Hundhausen et al., 2024). The less extreme biases in NUKLEUS compared to KIT-KLIWA, which can also be referred to as an ensemble of opportunity, confirm the importance of a systematic selection of the driving GCMs as carried out for the NUKLEUS ensemble (see Sect. 2.1.1).

Regarding annual mean precipitation, both ensembles exhibit predominantly wet biases, especially in mountainous regions. Moreover, the bias for ECE- and MPI-driven CCLM simulations are qualitatively and quantitatively similar in both ensembles. Interestingly, in KIT-KLIWA ECE- and HadGEM-driven simulations exhibit similar precipitation bias patterns. In NUKLEUS, the same applies for all RCM simulations driven by ECE and MIR, respectively. The RCMs appear to modulate the climatological precipitation bias pattern similarly for different GCMs, but the driving GCMs appear to have the dominant impact. In contrast, the near-surface air temperature bias of ECE and HadGEM in KIT-KLIWA are clearly different as well as for ECE-CCLM and MIR-CCLM in NUKLEUS. This suggests that similarities in precipitation bias patterns may rather be grounded in dynamic than thermodynamic reasons. Potential insight could be gained from a detailed analysis of seasonal mean biases and circulation weather types, which is beyond the scope of this study.

Overall, results between KIT-KLIWA and NUKLEUS agree well on climatological time scales. Although we do not present a systematic approach to disentangle the relative importance of GCMs and RCMs for the simulated climate, it is evident from the NUKLEUS ensemble that GCMs appear to be the more dominant factor. Nevertheless, the expansion to multiple RCMs in NUKLEUS provides valuable additional information beyond the single-model KIT-KLIWA ensemble, which allows growing confidence in the quality of the simulations and the derived climate change signals (cf. Beier et al., 2026) by attributing shares of the ensemble bandwidth to either GCMs or RCMs. A systematic investigation could, for example, be performed via the analysis of variance (Déqué et al., 2007). Moreover, from a practical point of view, multi-model RCM simulations could be considered as multiple realizations of the regional climate determined by the same GCM, and eventually be pooled together to artificially create longer time series for further analysis, such as extreme value statistics of very rare events, as, for example, done by Voit et al. (2026). This, however, would first require a more detailed analysis of the homogeneity of the resulting pooled data sets and implications for the validity of the underlying assumptions for statistical analysis.

5.2 EURO-CORDEX

In order to additionally provide a comparison of NUKLEUS to an ensemble that covers entire Germany, we use the EURO-CORDEX ensemble (Jacob et al., 2014), for which simulations were conducted on a horizontal resolution of 12 km covering

https://doi.org/10.5194/egusphere-2026-2517
Preprint. Discussion started: 11 June 2026

entire Europe (EUR-12 domain). The EURO-CORDEX ensemble consists of 11 RCMs downscaling eight CMIP5 GCMs over Europe. Since GCMs from the same "model-families" as the GCMs applied in NUKLEUS were also downscaled in EURO-CORDEX using the RCMs CCLM and REMO, this allows for a direct comparison of NUKLEUS to a subset of the EURO-CORDEX ensemble, although different model version were applied for GCMs and RCMs in the two ensembles. Vautard et al. (2021) compared the resulting 55 GCM-RCM combinations over the period 1981—2010 to an observational data set for daily near-surface temperature and precipitation, and ERA5 for wind.

Regarding temperature, maximum cold biases in winter in EURO-CORDEX reach up to –5 °C in the (Pre-)Alpine area, while the NUKLEUS ensemble shows a weak to moderate warm bias in all simulations. During summer, the NUKLEUS ensemble members exhibit less pronounced cold biases than found in the EURO-CORDEX ensemble, while there are similarly strong warm biases in both ensembles, which are found in NUKLEUS in the MIR-driven simulations, especially MIR-REMO. The entire EURO-CORDEX ensemble exhibits a larger range of biases for the mid-Europe (ME) prudence region than NUKLEUS for Germany during both winter and summer. From both ensembles, it is evident that the driving GCMs seem to be more dominant for simulated near-surface temperature than the RCMs. Deeper insight could here be gained by an analysis of variance applied to the ensemble members, as, for example, done by Déqué et al. (2007).

Regarding precipitation, EURO-CORDEX and NUKLEUS exhibit more intense wet than dry biases during winter and summer, with notably less pronounced dry biases in NUKLEUS during winter. During summer, the 95th percentile (and median) of the EURO-CORDEX ensemble bias is remarkably low in the Pre-Alpine region, which coincides with rather small wet or even weak dry biases in seven of nine NUKLEUS simulations.

Overall, the comparison of the convection-permitting NUKLEUS simulations against the coarser-scale EURO-CORDEX ensemble exhibits indications of an added value of the high-resolution CPM simulations, such as an improved representation of near-surface temperature and precipitation above complex orography, manifesting in slightly reduced biases due to the higher spatial resolution.

6 Analysis of bias-corrected NUKLEUS data

6.1 Basic meteorological variables and climate indices

Given the results presented in the preceding sections, bias correction of the NUKLEUS data may be required for subsequent applications. Due to the choice of the specific QDM method (see Sect. 2.4), the range of each simulated daily time series of the four basic meteorological variables (daily precipitation totals, and daily mean, minimum, and maximum 2 m temperature) for each model and at each grid point is constrained to the range of the HYRAS reference data by design (not shown). As a consequence, climatological analyses, such as the 30-year mean or annual cycles, of the bias-corrected simulation outputs agree exactly with the reference data set for single grid points, as well as for spatially aggregated measures (not shown). However, the temporal sequence is not affected by the QDM approach.

For the derived ETCCDI indices, bias correction yields a significant reduction in biases for threshold-based indices, while the improvement is more moderate for percentile-based indices. For threshold-based indices, the bias correction successfully

https://doi.org/10.5194/egusphere-2026-2517
Preprint. Discussion started: 11 June 2026

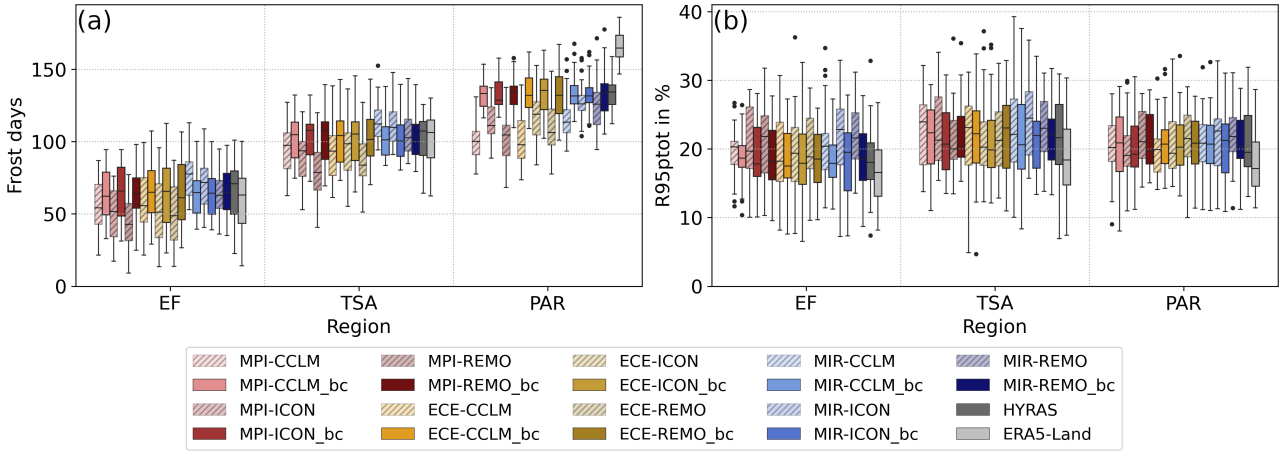

Figure 17. Comparison of the box plots before (hatched) and after (filled) the bias correction (bc) of (a) frost days, and (b) the contribution of very wet days with daily totals above the 95th percentile to the total annual precipitation (R95ptot) for the pilot regions EF, TSA, and PAR. Given are HYRAS (dark gray), ERA5-Land (light gray), and the NUKLEUS ensemble: reddish colors mark the CPM simulations driven by MPI, yellowish colors those driven by ECE, and blueish those driven by MIR. The center line indicates the median, the box edges the interquartile range (IQR), and the whiskers extend to 1.5 × IQR. The dots mark outliers.

removes the climatological bias, making the corrected mean identical to HYRAS (not shown), while largely preserving the simulated interannual variability. This is exemplified for frost days in Fig. 17a. The effect is less pronounced for percentile-based indices such as R95ptot, as shown in Fig. 17b, due to their relative definition, which inherently limits the degree of bias reduction.

6.2 Event-based analyses

Due to the grid point-wise application of the QDM, the conservation of spatial structures is not guaranteed, and locally the bias correction spuriously introduces strong spatial gradients. Figure 18 shows the daily precipitation sum simulated by ECE-CCLM on four consecutive days prior (a–d) and after the bias correction (e–h). After bias correction, there are sharp spatial gradients in the precipitation field in Eastern Germany as on 22 (Fig. 18f) and 24 August 1962 (Fig. 18h). Thus, for event-based investigations that require spatially coherent precipitation fields, such as using the precipitation data as input for hydrological models, the here-chosen QDM approach does not necessarily yield reasonable results.

This spatial non-coherence of the precipitation fields resulting from the bias correction also impacts the statistics of extreme precipitation events classified via the precipitation severity index (PSI; Sect. 2.5.2). Table 3 exemplary lists the six most extreme precipitation events detected from the daily precipitation totals simulated by ECE-CCLM prior to the bias correction including the associated PSI and the ranking by PSI (original) along with the PSI and ranking of the corresponding events after bias correction. From Table 3, it is evident that, for example, the 24 August 1962 event, for which the associated daily precipitation fields are shown in Fig. 18, is ranked as the second most extreme event prior to bias correction and the most extreme event

https://doi.org/10.5194/egusphere-2026-2517
Preprint. Discussion started: 11 June 2026

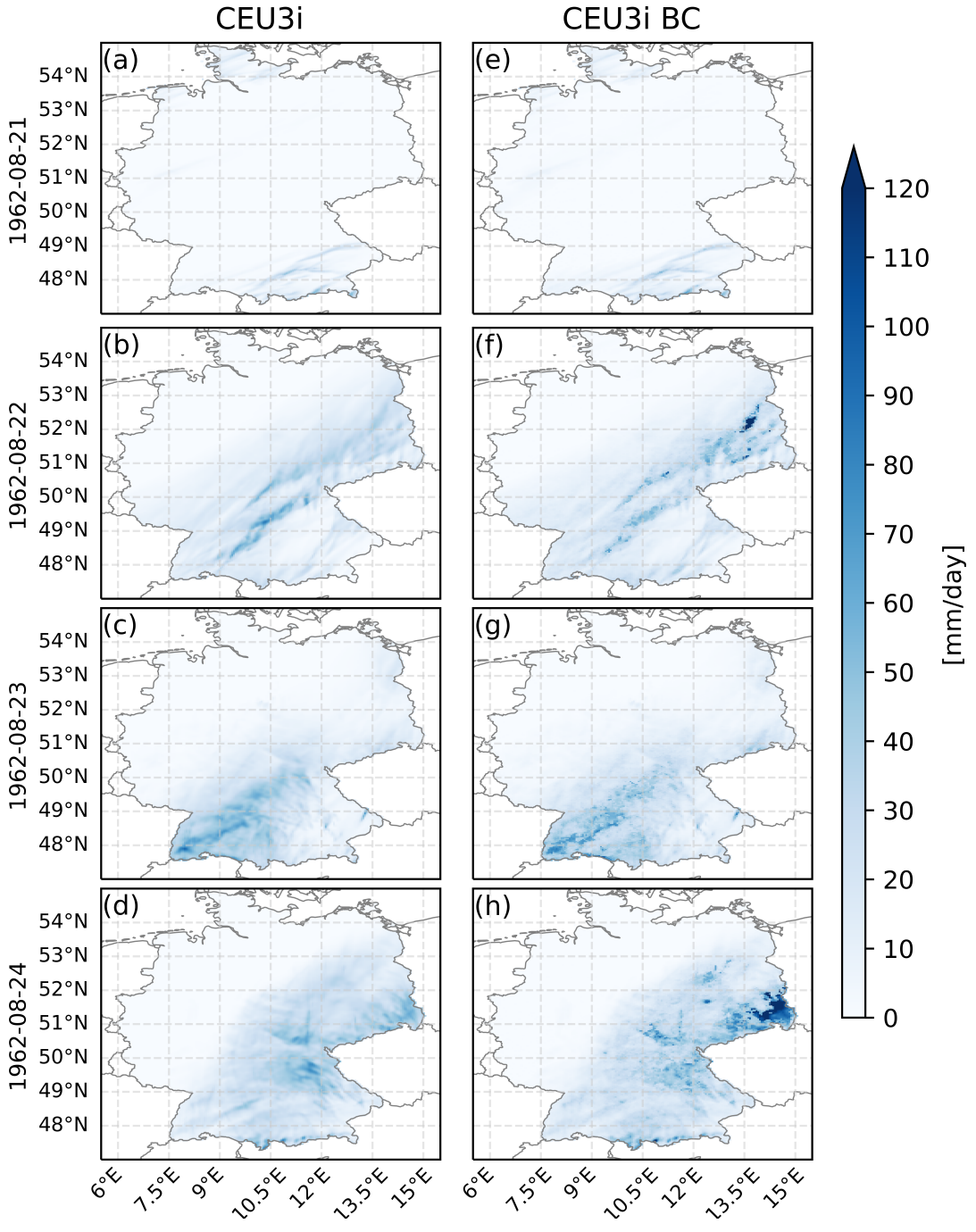

Figure 18. Comparison of daily precipitation totals simulated by ECE-CCLM prior (a–d) and after (e–h) bias correction for four consecutive days of an extreme precipitation event in late August 1962 (21–24 August; from top to bottom) detected with the PSI method.

https://doi.org/10.5194/egusphere-2026-2517
Preprint. Discussion started: 11 June 2026

Table 3. Comparison of the six most extreme precipitation events, as ranked by the precipitation severity index (PSI), from the original uncorrected (uc) ECE-CCLM simulation with the PSI values and corresponding ranks of the same events within the bias-corrected (bc) data set.

Date	Original (uc)		Bias-corrected (bc)	
(year-month-day)	PSI_{uc}	$Rank_{uc}$	PSI_{bc}	$Rank_{bc}$
1967-06-23	0.67	1	0.63	2
1962-08-24	0.58	2	0.72	1
1961-07-05	0.53	3	0.49	3
1976-04-25	0.51	4	0.41	11
1986-12-31	0.49	5	0.47	4
1967-06-22	0.47	6	0.47	5

afterward. Overall, there are negligible (e.g., 22 June 1967) to considerable (e.g., 24 August 1962) differences in the PSI for single events. Most of the ranks do not agree between original and bias-corrected data. However, the top five events detected in the bias-corrected data are contained in the top six of the original data. Overall, this emphasizes that the chosen QDM approach clearly impacts single precipitation events and does not necessarily provide a suitable data set for event-based analyses. Yet, the impact of the bias correction method may be within an acceptable range for the derivation of highly aggregated statistics over numerous precipitation events, in case it is required to derive such statistics from bias-corrected data.

7 Summary and Discussion

In this study, we analyzed the simulations of the historical reference period 1961–1990 of the NUKLEUS ensemble, the first regional kilometer-scale convection-permitting multi-model climate ensemble for Germany. The NUKLEUS ensemble consists of nine members: three regional climate models (RCMs) were used to downscale three global climate models (GCMs) from the CMIP6 ensemble to a horizontal grid resolution of 3 km. The analysis covered the statistical representation of basic meteorological variables (temperature, wind, precipitation) from annual to hourly time scales, and a selection of application-relevant climate indices from ETCCDI (Karl et al., 1999). Comparison was made to observation-based and reanalysis data sets for Germany and six pilot regions representing different topographic, climatic, and land use conditions, as well as socio-economic challenges for climate adaptation. A bias correction using the quantile delta mapping (QDM; Cannon et al., 2015) approach was performed and conclusions regarding its applicability in downstream applications were drawn.

The following main conclusions can be drawn from the presented results, also with respect to the overall aim of NUKLEUS of providing high-resolution and quality data for past and future climate conditions to support local adaptation initiatives:

https://doi.org/10.5194/egusphere-2026-2517
Preprint. Discussion started: 11 June 2026

1. The NUKLEUS ensemble is capable of reasonably reproducing the spatial and temporal characteristics of the 2 m temperature, 10 m wind speed, and precipitation over Germany on annual to hourly time scales in comparison with the used reference data sets HYRAS and ERA5-Land. Some of the NUKLEUS simulations exhibit considerable warm and cold biases, especially during winter and summer. Nearly all NUKLEUS simulations exhibit a wet bias for most geographic regions and seasons.

2. Extreme climate indices using percentile-based thresholds are well represented in the NUKLEUS ensemble compared to HYRAS, with better representation of temperature-related indices than precipitation-related indices. Indices using fixed numerical thresholds show an overestimation for precipitation and warm temperature-based quantities, and an underestimation of cold temperature-based quantities.

3. The NUKLEUS ensemble substantially expands the currently available RCM-based climate information over Central Europe beyond the EURO-CORDEX ensemble due to higher spatial resolution, and the single-model CPM ensemble KIT-KLIWA due to the multi-model CPM design of NUKLEUS including a systematic GCM selection.

4. The applied quantile delta mapping (QDM) bias correction approach successfully removes the climatological bias of daily temperature and precipitation. Significant improvement due to the QDM is found for indices using fixed numerical thresholds. For event-based analyses the QDM reveals shortcomings by impacting the spatial structure of precipitation fields, for example, by creating strong spatial gradients.

Overall, the NUKLEUS ensemble exhibits moderate warm and cold biases of near-surface air temperature and a predominantly wet bias of precipitation against HYRAS. The temperature biases are expected to originate to a considerable extent from the driving GCMs, as the corresponding global simulations are “running free”, and therefore are not expected to match the observed phases of large scale (multi-)decadal variability determining central European climate, such as the North Atlantic Oscillation and the Atlantic Multidecadal Oscillation. This becomes particular relevant when focussing on a specific short period, only, such as the 30-year historical reference period. Hence, this feature of the GCMs leads to large regional differences in near-surface air temperature, that are already substantially reduced by the applied regional climate models at the intermediate downscaling step on the 12 km EUR-12 domain (Cusinato et al., 2026). Moreover, the simulated single-year annual or seasonal mean temperatures in the here-studied 3 km CEU-3 simulations are contained to a large extent within the observed range for all pilot regions and seasons. Furthermore, the bias of near-surface air temperature for all seasons, regions, and GCM-RCM pairs is smaller than the corresponding observed range of interannual or interseasonal variability. This supports the expectation that a considerable share of these temperature biases originate from uncertainties in long-term and large-scale climate variability propagating from the free-running forcing GCM into the RCM simulations.

For precipitation, likewise a large extent of the simulated single-year annual or seasonal mean precipitation sums is contained within the observed range. However, simulations exhibit a clear tendency to higher precipitation sums, except for summer, representing the aforementioned systematic wet bias, especially in mountainous regions, which is a known issue of CPMs (Prein et al., 2015; Hundhausen et al., 2024). Similar systematic and partly substantial biases were found for 10 m wind speed

https://doi.org/10.5194/egusphere-2026-2517
Preprint. Discussion started: 11 June 2026

and precipitation-based extreme climate indices. While these systematic biases of precipitation and 10 m wind speed may partly originate from model deficiencies, they may also contain large contributions from errors in the applied reference data sets with known shortcomings, such as the underestimation of precipitation measurements by ground-based gauges or the low spatial resolution of reanalysis data (Vautard et al., 2021). Hence, the biases found within this study are not expected to originate exclusively from model deficiencies.

The temperature and precipitation biases of single members of the NUKLEUS ensemble with respect to HYRAS are less pronounced than biases found in the single-model KIT-KLIWA ensemble, indicating the importance of a systematic GCM selection as carried out in NUKLEUS. Furthermore, smaller biases of temperature and precipitation in regions of complex terrain provide indications of an added value of the high-resolution NUKLEUS simulations compared to the coarser-scale EURO-CORDEX ensemble.

Overall, the biases exhibited by the NUKLEUS simulations appear to be within reasonable and expected ranges. Nevertheless, the biases are still too large for direct downstream applications of the simulation output, such as threshold-based extreme climate index derivation or impact modeling. Hence, a bias correction is required in these cases. Within this study, the standard quantile delta mapping (QDM; Cannon et al., 2015) approach was applied. This approach uses the same number of quantiles as available time steps, which means, it results in a one-to-one mapping of simulated values to observed values during the historical period. As a consequence, biases are completely eliminated on climatological time scales. The standard QDM approach is therefore a helpful and straightforward method for deriving climate change signals as presented in Beier et al. (2026). The main limitation of the standard QDM approach is the inability to preserve spatially coherent structures often required as input for impact models (Allard et al., 2025). This limitation could be addressed using a method that considers the spatial coherence of the physical variables, such as a multivariate bias correction (e.g., Vrac and Friederichs, 2015; Allard et al., 2025) or machine learning techniques (e.g., Pan et al., 2021). Another option for improvement would be the application of a more flexible bias correction procedure. Pinto et al. (2026), for example, used 100 quantiles for temperature and 1000 quantiles for precipitation, while Ehmele et al. (2022) used parameterized probability density functions (pdfs). However, this results in a non-zero residual bias on climatological time scales, with a substantial warm bias remaining in one case (HadGEM) in Pinto et al. (2026). In addition, parameterized pdfs may not be sufficiently strict for downstream applications (non-zero residual biases) and are also not easily transferable to climate projections. Thus, the choice of the bias correction method should be based on the desired applications.

Based on our analyses and the comparison with existing ensembles, we conclude that the NUKLEUS ensemble reasonably represents the past climate and is therefore considered as a useful data set for analyzing future projections of the central European climate. Especially in combination with suitable bias correction methods that are carefully selected for specific downstream applications, valuable action-oriented climate information can be derived from the NUKLEUS ensemble. Further discussion of the interplay of bias correction and the added value of high spatial resolution in the NUKLEUS simulations (CEU-3) compared to the parent intermediate resolution (EUR-12) is planned for an accompanying study. The resulting climate change signals for basic meteorological variables and selected extreme climate indices under 2 K and 3 K global warming are investigated in the accompanying study by Beier et al. (2026).

https://doi.org/10.5194/egusphere-2026-2517
Preprint. Discussion started: 11 June 2026

Code and data availability. The ICON release icon-2.6.5 was used for the for the ICON simulations. The access to the applied ICON model version is license-restricted and the model code may not be made publicly available. To obtain the model code, the user needs to obtain access to the ICON-gitlab repository hosted by the German Climate Computing Center (Deutsches Klimarechenzentrum; https://gitlab.dkrz.de/icon/icon). The execution of the job workflow for ICON was managed using SPICE - Starter Package for ICON-CLM Experiments, specifically the version 2.1 released in January 2022, which is publicly available on Zenodo (https://zenodo.org/records/6838984; Rockel and Geyer, 2022b). The final release of COSMO (cosmo6.0) was applied. The documentation of the COSMO model is developed by the COSMO Consortium and consists of user guide and scientific documentation permanently available at https://www.dwd.de/EN/ourservices/cosmo_documentation/cosmo_documentation.html (last access: 12 January 2026). The COSMO-CLM model is free of charge for all research applications; however, access is license-restricted: https://www.cosmo-model.org/content/consortium/licencing.htm (last access: 12 January 2026). To download, the user needs to become a member of the CLM-Community or the respective institute needs to hold an institutional license. The execution of the job workflow for COSMO was managed using the Starter Package for COSMO-CLM Experiments, specifically the version 5.0 released in February 2022, which is publicly available on Zenodo (https://doi.org/10.5281/zenodo.7290478; Rockel and Geyer, 2022a). The sources for the REMO model are available on request from the Climate Service Center Germany (contact@remo-rcm.de). Open access is not possible due to licensing limitations coming from the legacy code within REMO. The version used in this work is saved and archived on Zenodo (https://doi.org/10.5281/zenodo.15679389). The NUKLEUS data is available at the German Climate Computing Center (DKRZ), but requires a login: https://www-regiklim.dkrz.de. Further information on the available data can be found at: https://ch1187.gitlab-pages.dkrz.de/Information/Data.html. An openly available access is planned for September 2026 in a data portal at DKRZ that is part of the funding of the NUKLEUS project and currently under development. A subset of the HYRAS-DE dataset version 5.0 interpolated to the curvilinear rotated CEU-3 grid used within this study is publicly available under https://www.radar-service.eu/radar/en/dataset/gur5c2ujfp2cj5na?token=uJxgHeCzcyrgZVtPWWcy. Please note that a more recent version of HYRAS-DE is freely available for research at the Open Data Portal of Germany's National Meteorological Service DWD (https://opendata.dwd.de/climate_environment/CDC/grids_germany/daily/hyras_de/, last access: 3 June 2026). The technical description of the HYRAS datasets can be found under https://www.dwd.de/hyras (last access: 3 June 2026). The forcing data from the used GCMs is available under https://doi.org/10.22033/ESGF/CMIP6.6594 for MPI-ESM1-2-HR, https://doi.org/10.22033/ESGF/CMIP6.5603 for MIROC6, and https://doi.org/10.22033/ESGF/CMIP6.4706 for EC-Earth3-Veg. The reanalyses data of ERA5 (https://www.doi.org/10.24381/cds.adbb2d47) and ERA5-Land (https://www.doi.org/10.24381/cds.e2161bac) can be downloaded after registration from the Copernicus Climate Change Service (C3S) Climate Data Store: https://cds.climate.copernicus.eu.

Author contributions. The conceptualization of this study was developed by CBr, FE, and HF. The selection of suitable GCMs was coordinated by HF, KK, and KS. The simulations were conducted by HF, BG, TF, and KK. The bias correction was conducted by EE and EX with contributions from CBr and FE. Plotting routines and figure production were done by CBr, FE, CBe, and MH. CBr conducted the analysis of biases, variability, and PSI with contributions from EE. FE conducted the analyses of pdfs, climate indices and annual/diurnal cycles with contributions from CBe and MH. The paper writing was done by CBr and FE with contributions from CBe and EE. The overall management of the collaboration was done by KS and JGP. All authors contributed with fruitful discussions and text revisions.

Competing interests. The authors declare that they have no conflict of interest.

https://doi.org/10.5194/egusphere-2026-2517
Preprint. Discussion started: 11 June 2026

Acknowledgements. This work used resources of the German Climate Computing Center (DKRZ) granted by its Scientific Steering Committee (WLA) under project IDs bg1187 and bb1203. We thank DKRZ for providing the computing time and storage resources, and also for granting access to some of the used data sets via the central data pool. We also thank the CLM community for providing GCM data. We acknowledge the ERA5 and ERA5-Land data set from the Copernicus Climate Change Service (C3S) and ECA&D Climate Data Store (CDS; https://www.ecad.eu, last access: 20 March 2026). In addition, we thank the Germany's National Meteorological Service (Deutscher Wetterdienst; DWD) for providing the HYRAS data set. We further thank Julia Moemken (formerly KIT) for contributing to the GCM selection and bias analyses, Michael Woldt (BTU Cottbus-Senftenberg), who supported the ICON-CLM simulations and data post-processing, and Burkhardt Rockel (Hereon) and Ronny Petrik (German Navy Headquarters), who also contributed to the GCM selection. JGP thanks the AXA Research Fund.

https://doi.org/10.5194/egusphere-2026-2517
Preprint. Discussion started: 11 June 2026

References

Alexander, L. and Herold, N.: ClimPACT2: Indices and software, accessed April 2025, https://hdl.handle.net/10013/epic.94f52968-eeed-4766-9285-5c3466c98932, 2016.

Allard, D., Vrac, M., François, B., and García de Cortázar-Atauri, I.: Assessing multivariate bias corrections of climate simulations on various impact models under climate change, Hydrol. Earth Syst. Sci., 29, 4711–4738, https://doi.org/10.5194/hess-29-4711-2025, 2025.

Baldauf, M., Seifert, A., Förstner, J., Majewski, D., Raschendorfer, M., and Reinhardt, T.: Operational Convective-Scale Numerical Weather Prediction with the COSMO Model: Description and Sensitivities, Mon. Weather Rev., 139, 3887–3905, https://doi.org/10.1175/MWR-D-10-05013.1, 2011.

Ban, N., Caillaud, C., Coppola, E., Pichelli, E., Sobolowski, S., Adinolfi, M., Ahrens, B., Alias, A., Anders, I., Bastin, S., Belušić, D., Berthou, S., Brisson, E., Cardoso, R. M., Chan, S. C., Christensen, O. B., Fernández, J., Fita, L., Frisius, T., Gašparac, G., Giorgi, F., Goergen, K., Haugen, J. E., Hodnebrog, Ø., Kartsios, S., Katragkou, E., Kendon, E. J., Keuler, K., Lavin-Gullon, A., Lenderink, G., Leutwyler, D., Lorenz, T., Maraun, D., Mercogliano, P., Milovac, J., Panitz, H.-J., Raffa, M., Remedio, A. R., Schär, C., Soares, P. M. M., Srnec, L., Steensen, B. M., Stocchi, P., Tölle, M. H., Truhetz, H., Vergara-Temprado, J., de Vries, H., Warrach-Sagi, K., Wulfmeyer, V., and Zander, M. J.: The first multi-model ensemble of regional climate simulations at kilometer-scale resolution, part I: evaluation of precipitation, Clim. Dynam., 57, 275–302, https://doi.org/10.1007/s00382-021-05708-w, 2021.

Barriopedro, D., García-Herrera, R., and Trigo, R. M.: Application of blocking diagnosis methods to general circulation models. Part I: A novel detection scheme, Climate dynamics, 35, 1373–1391, https://doi.org/10.1007/s00382-010-0767-5, 2010.

Bechtold, P., Koehler, M., Jung, T., Doblas-Reyes, F., Leutbecher, M., Rodwell, M. J., Vitart, F., and Balsamo, G.: Advances in simulating atmospheric variability with the ECMWF model: From synoptic to decadal time-scales, Q. J. R. Meteorol. Soc., 134, 1337–1351, https://doi.org/10.1002/qj.289, 2008.

Beier, C., Ziegler, K., Paeth, H., Pinto, J. G., Sieck, K., Buntemeyer, L., Geyer, B., Xoplaki, E., Espitia, E., Braun, C., Ehmele, F., Feldmann, H., Kadow, C., and Trachte, K.: NUKLEUS - A First Convection Permitting Multi-model Ensemble for Germany: Assessment of future changes in temperature and precipitation extremes, under review at J. Climate, https://doi.org/10.1175/JCLI-D-25-0613, 2026.

Bell, B., Hersbach, H., Simmons, A., Berrisford, P., Dahlgren, P., Horányi, A., Muñoz-Sabater, J., Nicolas, J., Radu, R., Schepers, D., et al.: The ERA5 global reanalysis: Preliminary extension to 1950, Q. J. R. Meteorol. Soc., 147, 4186–4227, https://doi.org/10.1002/qj.4174, 2021.

Berg, P., Feldmann, H., and Panitz, H.-J.: Bias correction of high resolution regional climate model data, J. Hydrol., 448, 80–92, https://doi.org/10.1016/j.jhydrol.2012.04.026, 2012.

Brunner, L., Pendergrass, A., Lehner, F., Merrifield, A., Lorenz, R., and Knutti, R.: Reduced global warming from CMIP6 projections when weighting models by performance and independence, Earth Syst. Dynam., 11, 995–1012, https://doi.org/10.5194/esd-11-995-2020, 2020.

Caldas-Alvarez, A., Feldmann, H., Lucio-Eceiza, E., and Pinto, J. G.: Convection-parameterized and convection-permitting modelling of heavy precipitation in decadal simulations of the greater Alpine region with COSMO-CLM, Weather Clim. Dyn., 4, 543—-565, https://doi.org/10.5194/wcd-4-543-2023, 2023.

Cannon, A. J., Sobie, S. R., and Murdock, T. Q.: Bias Correction of GCM Precipitation by Quantile Mapping: How Well Do Methods Preserve Changes in Quantiles and Extremes?, J. Climate, 28, 6938–6959, https://doi.org/10.1175/JCLI-D-14-00754.1, 2015.

Climpact: Climpact Indices, Accessed 22 October 2025, https://climpact-sci.org/indices/, 2024.

https://doi.org/10.5194/egusphere-2026-2517
Preprint. Discussion started: 11 June 2026

Coppola, E., Sobolowski, S., Pichelli, E., Raffaele, F., Ahrens, B., Anders, I., Ban, N., Bastin, S., Belda, M., Belusic, D., Caldas-Alvarez, A., Cardoso, R. M., Davolio, S., Dobler, A., Fernandez, J., Fita, L., Fumiere, Q., Giorgi, F., Goergen, K., Güttler, I., Halenka, T., Heinzeller, D., Hodnebrog, Ø., Jacob, D., Kartsios, S., Katragkou, E., Kendon, E., Khodayar, S., Kunstmann, H., Knist, S., Lavín-Gullón, A., Lind, P., Lorenz, T., Maraun, D., Marelle, L., van Meijgaard, E., Milovac, J., Myhre, G., Panitz, H.-J., Piazza, M., Raffa, M., Raub, T., Rockel, B., Schär, C., Sieck, K., Soares, P. M. M., Somot, S., Srnec, L., Stocchi, P., Tölle, M. H., Truhetz, H., Vautard, R., de Vries, H., and Warrach-Sagi, K.: A first-of-its-kind multi-model convection permitting ensemble for investigating convective phenomena over Europe and the Mediterranean, Clim. Dynam., 55, 3–34, https://doi.org/10.1007/s00382-018-4521-8, 2020.

Cusinato, E., Feldmann, H., Geyer, B., Ludwig, P., Trachte, K., and G., P. J.: From Global to Regional Climate Models: Consistency Assessment of the Hydrological Cycle, under review at Clim. Dynam., 2026.

Dai, A.: The diurnal cycle from observations and ERA5 in precipitation, clouds, boundary layer height, buoyancy, and surface fluxes, Clim. Dynam., https://doi.org/10.1007/s00382-024-07182-6, 2024.

Deutscher Wetterdienst: Klimastatusbericht 2002, Gesamtausgabe, https://www.dwd.de/DE/leistungen/klimastatusbericht/publikationen/ksb_2002.pdf, online verfügbar, 2003.

Doury, A., Somot, S., Gadat, S., Ribes, A., and Corre, L.: Regional climate model emulator based on deep learning: concept and first evaluation of a novel hybrid downscaling approach, Clim. Dynam., 60, 1751–1779, https://doi.org/10.1007/s00382-022-06343-9, 2023.

Dutra, E., Muñoz-Sabater, J., Boussetta, S., Komori, T., Hirahara, S., and Balsamo, G.: Environmental Lapse Rate for High-Resolution Land Surface Downscaling: An Application to ERA5, Earth and Space Sci., 7, e2019EA000 984, https://doi.org/10.1029/2019EA000984, _eprint: https://agupubs.onlinelibrary.wiley.com/doi/pdf/10.1029/2019EA000984, 2020.

Déqué, M., Rowell, D. P., Lüthi, D., Giorgi, F., Christensen, J. H., Rockel, B., Jacob, D., Kjellström, E., de Castro, M., and van den Hurk, B.: An intercomparison of regional climate simulations for Europe: assessing uncertainties in model projections, Clim. Change, 81, 53—-70, https://doi.org/10.1007/s10584-006-9228-x, 2007.

EC-Earth Consortium (EC-Earth): EC-Earth-Consortium EC-Earth3-Veg model output prepared for CMIP6 ScenarioMIP ssp370, https://doi.org/10.22033/ESGF/CMIP6.4886, 2019.

Ehmele, F., Kautz, L.-A., Feldmann, H., and Pinto, J. G.: Long-term variance of heavy precipitation across central Europe using a large ensemble of regional climate model simulations, Earth Syst. Dynam., 11, 469–490, https://doi.org/10.5194/esd-11-469-2020, 2020.

Ehmele, F., Kautz, L.-A., Feldmann, H., He, Y., Kadlec, M., Kelemen, F. D., Lentink, H. S., Ludwig, P., Manful, D., and Pinto, J. G.: Adaptation and application of the large LAERTES-EU regional climate model ensemble for modeling hydrological extremes: a pilot study for the Rhine basin, Nat. Hazards Earth Syst. Sci., 22, 677–692, https://doi.org/10.5194/nhess-22-677-2022, 2022.

Eyring, V., Bony, S., Meehl, G. A.and Senior, C. A., Stevens, B., Stouffer, R. J., and Taylor, K. E.: Overview of the Coupled Model Intercomparison Project Phase 6 (CMIP6) experimental design and organization, Geosci. Model Dev., 9, 1937–1958, https://doi.org/10.5194/gmd-9-1937-2016, 2016.

Fernandez-Granja, J. A., Casanueva, A., Bedia, J., and Fernandez, J.: Improved atmospheric circulation over Europe by the new generation of CMIP6 earth system models, Clim. Dynam., 56, 3527–3540, https://doi.org/10.1007/s00382-021-05652-9, 2021.

Fowler, H. J., Ali, H., Allan, R. P., Ban, N., Barbero, R., Berg, P., Blenkinsop, S., Cabi, N. S., Chan, S., Dale, M., Dunn, R. J. H., Ekström, M., Evans, J. P., Fosser, G., Golding, B., Guerreiro, S. B., Hegerl, G. C., Kahraman, A., Kendon, E. J., Lenderink, G., Lewis, E., Li, X., O'Gorman, P. A., Orr, H. G., Peat, K. L., Prein, A. F., Pritchard, D., Schär, C., Sharma, A., Stott, P. A., Villalobos-Herrera, R., Villarini, G., Wasko, C., Wehner, M. F., Westra, S., and Whitford, A.: Towards advancing scientific knowledge of climate change impacts on short-

https://doi.org/10.5194/egusphere-2026-2517
Preprint. Discussion started: 11 June 2026

duration rainfall extremes, Philosophical Transactions of the Royal Society A: Mathematical, Physical and Engineering Sciences, 379, 20190 542, https://doi.org/10.1098/rsta.2019.0542, 2021.

Fünfgeld, H., Fila, D., and Dahlmann, H.: Upscaling climate change adaptation in small- and medium-sized municipalities: current barriers and future potentials, Current Opinion in Environmental Sustainability, 61, 101 263, https://doi.org/10.1016/j.cosust.2023.101263, 2023.

Fünfgeld, H., Christen, A., Briegel, F., Schrodi, S., Speidel, A., Felder, C., Hoffmann, J., Irscheid, L., Merkle, D., Meyer, J., Schindler, D., Wehrle, J., and Zengerling, C.: Optimizing urban greening and densification in the context of outdoor heat: Opportunities for AI-supported urban adaptation, Landscape and Urban Planning, 268, 105 574, https://doi.org/10.1016/j.landurbplan.2025.105574, 2026.

Giorgi, F. and Gutowski, W. J.: Regional Dynamical Downscaling and the CORDEX Initiative, Ann. Rev. Environ. Resour., 40, 467–490, https://doi.org/10.1146/annurev-environ-102014-021217, 2015.

Giorgi, F., Jones, C., and Asrar, G.: Addressing climate information needs at the regional level: The CORDEX framework, WMO Bull, 53, 175–183, 2009.

Grasselt, R., Schuettemeyer, D., Warrach-Sagi, K., Ament, F., and Simmer, C.: Validation of TERRA-ML with discharge measurements, Meteorologische Zeitschrift, 17, 763–773, 2008.

Gutiérrez, J. M., Maraun, D., Widmann, M., Huth, R., Hertig, E., Benestad, R., Roessler, O., Wibig, J., Wilcke, R., Kotlarski, S., San Martín, D., Herrera, S., Bedia, J., Casanueva, A., Manzanas, R., Iturbide, M., Vrac, M., Dubrovsky, M., Ribalaygua, J., Pórtoles, J., Räty, O., Räisänen, J., Hingray, B., Raynaud, D., Casado, M. J., Ramos, P., Zerenner, T., Turco, M., Bosshard, T., Štěpánek, P., Bartholy, J., Pongracz, R., Keller, D. E., Fischer, A. M., Cardoso, R. M., Soares, P. M. M., Czernecki, B., and Pagé, C.: An intercomparison of a large ensemble of statistical downscaling methods over Europe: Results from the VALUE perfect predictor cross-validation experiment, Int. J. Climatol., 39, 3750–3785, https://doi.org/https://doi.org/10.1002/joc.5462, 2019.

Gutowski Jr., W., Giorgi, F., Timbal, B., Frigon, A., Jacob, D., Kang, H.-S., Raghavan, K.and Lee, B., Lennard, C., Nikulin, G., O'Rourke, E., Rixen, M.and Solman, S., Stephenson, T., and Tangang, F.: WCRP COordinated Regional Downscaling EXperiment (CORDEX): a diagnostic MIP for CMIP6, Geosci. Model Dev., 9, 4087–4095, https://doi.org/10.5194/gmd-9-4087-2016, 2016.

Göttel, H.: Einfluss der nichthydrostatischen Modellierung und der Niederschlagsverdriftung auf die Ergebnisse regionaler Klimamodellierung, Ph.D. thesis, Max-Planck-Institut für Meteorologie, 2009.

Hersbach, H., Bell, B., Berrisford, P., Hirahara, S., Horányi, A., Muñoz-Sabater, J., Nicolas, J., Peubey, C., Radu, R., Schepers, D., Simmons, A., Soci, C., Abdalla, S., Abellan, X., Balsamo, G., Bechtold, P., Biavati, G., Bidlot, J., Bonavita, M., De Chiara, G., Dahlgren, P., Dee, D., Diamantakis, M., Dragani, R., Flemming, J., Forbes, R., Fuentes, M., Geer, A., Haimberger, L., Healy, S., Hogan, R. J., Hólm, E., Janisková, M., Keeley, S., Laloyaux, P., Lopez, P., Lupu, C., Radnoti, G., de Rosnay, P., Rozum, I., Vamborg, F., Villaume, S., and Thépaut, J.-N.: The ERA5 global reanalysis, Q. J. R. Meteorol. Soc., 146, 1999–2049, https://doi.org/10.1002/qj.3803, 2020.

Hundhausen, M., Feldmann, H., Laube, N., and Pinto, J. G.: Future heat extremes and impacts in a convection-permitting climate ensemble over Germany, Natural Hazards and Earth System Sciences, 23, 2873–2893, https://doi.org/10.5194/nhess-23-2873-2023, 2023.

Hundhausen, M., Feldmann, H., Kohlhepp, R., and Pinto, J. G.: Climate change signals of extreme precipitation return levels for Germany in a transient convection-permitting simulation ensemble, International Journal of Climatology, 44, 1454–1471, https://doi.org/10.1002/joc.8393, 2024.

Hyndman, R. J. and Fan, Y.: Sample Quantiles in Statistical Packages, The American Statistician, 50, 361–365, https://doi.org/10.1080/00031305.1996.10473566, 1996.

Ivanov, M. A., Luterbacher, J., and Kotlarski, S.: Climate model biases and modification of the climate change signal by intensity-dependent bias correction, J. Climate, 31, 6591–6610, https://doi.org/10.1175/JCLI-D-17-0765.1, 2018.

https://doi.org/10.5194/egusphere-2026-2517
Preprint. Discussion started: 11 June 2026

Jacob, D. and Podzun, R.: Sensitivity studies with the regional climate model REMO, Meteorol. Atmos. Phys., 63, 119–129, https://doi.org/https://doi.org/10.1007/BF01025368, 1997.

Jacob, D., Petersen, J., Eggert, B., Alias, A., Christensen, O. ø., Bouwer, L. M., Braun, A., Colette, A., Déqué, M., Georgievski, G., Georgopoulou, E., Gobiet, A., Menut, L., Nikulin, G., Haensler, A., Hempelmann, N., Jones, C., Keuler, K., Kovats, S., Kröner, N., Kotlarski, S., Kriegsmann, A., Martin, E., van Meijgaard, E., Moseley, C., Pfeifer, S., Preuschmann, S., Radermacher, C., Radtke, K., Rechid, D., Rounsevell, M., Samuelsson, P., Somot, S., Soussana, J.-F., Teichmann, C., Valentini, R., Vautard, R., Weber, B., and Yiou, P.: EURO-CORDEX: new high-resolution climate change projections for European impact research, Reg. Environ. Change, 14, 563–578, https://doi.org/10.1007/s10113-013-0499-2, 2014.

Janjic, Z. I., Gerrity, J. P., and Nickovic, S.: An alternative approach to nonhydrostatic modeling, Mon. Weather Rev., 129, 1164–1178, 2001.

Jones, P., Hulme, M., and Briffa, K.: A comparison of lamb circulation types with an objective classification scheme, Int. J. Climatol., 13, 655–663, https://doi.org/10.1002/joc.3370130606, 1993.

Jungclaus, J., Bittner, M., Wieners, K.-H., Wachsmann, F., Schupfner, M., Legutke, S., Giorgetta, M., Reick, C., Gayler, V., Haak, H., de Vrese, P., Raddatz, T., Esch, M., Mauritsen, T., von Storch, J.-S., Behrens, J., Brovkin, V., Claussen, M., Crueger, T., Fast, I., Fiedler, S., Hagemann, S., Hohenegger, C., Jahns, T., Kloster, S., Kinne, S., Lasslop, G., Kornblueh, L., Marotzke, J., Matei, D., Meraner, K., Mikolajewicz, U., Modali, K., Müller, W., Nabel, J., Notz, D., Peters-von Gehlen, K., Pincus, R., Pohlmann, H., Pongratz, J., Rast, S., Schmidt, H., Schnur, R., Schulzweida, U., Six, K., Stevens, B., Voigt, A., and Roeckner, E.: MPI-M MPI-ESM1.2-HR model output prepared for CMIP6 CMIP historical, https://doi.org/10.22033/ESGF/CMIP6.6594, 2019.

Kadow, C., Illing, S., Lucio-Eceiza, E., Bergemann, M., Ramadoss, M., Sommer, P., Kunst, O., Schartner, T., Pankatz, K., Grieger, J., Schuster, M., Richling, A., Thiemann, H., Kirchner, I., Rust, H., Ludwig, T., Cubasch, U., and Ulbrich, U.: Introduction to Freva - A Free Evaluation System Framework for Earth System Modeling, J. Open Res. Software, https://doi.org/10.5334/jors.253, 2021.

Karl, T. R., Nicholls, N., and Ghazi, A.: CLIVAR/GCOS/WMO Workshop on Indices and Indicators for Climate Extremes Workshop Summary, pp. 3–7, Springer Netherlands, Dordrecht, ISBN 978-94-015-9265-9, https://doi.org/10.1007/978-94-015-9265-9_2, 1999.

Kaspar, F., Imbery, F., and Friedrich, K.: Nutzung klimatologischer Referenzperioden ab 2021, Tech. rep., Deutscher Wetterdienst, https://www.dwd.de/DE/leistungen/besondereereignisse/verschiedenes/20210119_neue_referenzperiode.pdf?__blob=publicationFile&v=6, 2021.

Katragkou, E., Sobolowski, S. P., Teichmann, C., Solmon, F., Pavlidis, V., Rechid, D., Hoffmann, P., Fernandez, J., Nikulin, G., and Jacob, D.: Delivering an Improved Framework for the New Generation of CMIP6-Driven EURO-CORDEX Regional Climate Simulations, Bull. Am. Meteorol. Soc., 105, E962–E974, https://doi.org/10.1175/BAMS-D-23-0131.1, 2024.

Kendon, E. J., Roberts, N. M., Fosser, G., Martin, G. M., Lock, A. P., Murphy, J. M., Senior, C. A., and Tucker, S. O.: Greater Future U.K. Winter Precipitation Increase in New Convection-Permitting Scenarios, J. Climate, 33, 7303—-7318, https://doi.org/10.1175/JCLI-D-20-0089.1, 2020.

Kendon, E. J., Fischer, E. M., and Short, C. J.: Variability conceals emerging trend in 100yr projections of UK local hourly rainfall extremes, Nat. Commun., 14, 1133, https://doi.org/10.1038/s41467-023-36499-9, 2023.

Lanzante, J. R., Dixon, K. W., Nath, M. J., Whitlock, C. E., and Adams-Smith, D.: Some pitfalls in statistical downscaling of future climate, Bulletin of the American Meteorological Society, 99, 791–803, https://doi.org/10.1175/BAMS-D-17-0046.1, 2018.

Lucas-Picher, P., Argüeso, D., Brisson, E., Tramblay, Y., Berg, P., Lemonsu, A., Kotlarski, S., and Caillaud, C.: Convection-permitting modeling with regional climate models: Latest developments and next steps, WIRES Clim. Change, https://doi.org/10.1002/wcc.731, 2021.

https://doi.org/10.5194/egusphere-2026-2517
Preprint. Discussion started: 11 June 2026

Ludwig, P., Ehmele, F., Franca, M. J., Mohr, S., Caldas-Alvarez, A., Daniell, J. E., Ehret, U., Feldmann, H., Hundhausen, M., Knippertz, P., Küpfer, K., Kunz, M., Mühr, B., Pinto, J. G., Quinting, J., Schäfer, A. M., Seidel, F., and Wisotzky, C.: A multi-disciplinary analysis of the exceptional flood event of July 2021 in central Europe – Part 2: Historical context and relation to climate change, Nat. Hazards Earth Syst. Sci., 23, 1287–1311, https://doi.org/10.5194/nhess-23-1287-2023, 2023.

Maraun, D. and Widmann, M.: Statistical Downscaling and Bias Correction for Climate Research, Cambridge University Press, Cambridge, UK, https://doi.org/10.1017/9781107588783, 2018.

Maraun, D., Widmann, M., Gutiérrez, J. M., Kotlarski, S., Chandler, R. E., Hertig, E., Wibig, J., Huth, R., and Wilcke, R. A. I.: VALUE: A framework to validate downscaling approaches for climate change studies, Earth's Future, 3, 1–14, https://doi.org/10.1002/2014EF000259, 2015.

Masato, G., Hoskins, B. J., and Woollings, T.: Wave-breaking characteristics of Northern Hemisphere winter blocking: A two-dimensional approach, Journal of climate, 26, 4535–4549, https://doi.org/10.1175/JCLI-D-12-00240.1, 2013.

Masson-Delmotte, V., Zhai, P., Pirani, A., Connors, S., Péan, C., Berger, S., Caud, N., Chen, Y., Goldfarb, L., Gomis, M., Huang, M., Leitzell, K., Lonnoy, E., Matthews, J., Maycock, T., Waterfield, T., Yelekçi, O., Yu, R., and Zhou, B., eds.: Climate Change 2021: The Physical Science Basis. Contribution of Working Group I to the Sixth Assessment Report of the Intergovernmental Panel on Climate Change, Cambridge University Press, Cambridge, United Kingdom and New York, NY, USA, https://doi.org/10.1017/9781009157896, Intergovernmental Panel on Climate Change (IPCC), 2021.

Measham, T. G., Preston, B. L., Smith, T. F., Brooke, C., Gorddard, R., Withycombe, G., and Morrison, C.: Adapting to climate change through local municipal planning: barriers and challenges, Mitigation and Adaptation Strategies for Global Change, 16, 889–909, https://doi.org/10.1007/s11027-011-9301-2, 2011.

Mironov, D. V.: Parameterization of lakes in numerical weather prediction. Description of a lake model, Tech. Rep. 11, Consortium for Small-Scale Modelling, https://doi.org/10.5676/DWD_pub/nwv/cosmo-tr_11, 2008.

Mohr, S., Ehret, U., Kunz, M., Ludwig, P., Caldas-Alvarez, A., Daniell, J. E., Ehmele, F., Feldmann, H., Franca, M. J., Gattke, C., Hundhausen, M., Knippertz, P., Küpfer, K., Mühr, B., Pinto, J. G., Quinting, J., Schäfer, A. M., Scheibel, M., Seidel, F., and Wisotzky, C.: A multi-disciplinary analysis of the exceptional flood event of July 2021 in central Europe – Part 1: Event description and analysis, Nat. Hazards Earth Syst. Sci., 23, 525–551, https://doi.org/10.5194/nhess-23-525-2023, 2023.

Molina, M. O., Careto, J. M., Gutiérrez, C., Sánchez, E., Goergen, K., Sobolowski, S., Coppola, E., Pichelli, E., Ban, N., Belušić, D., Short, C., Caillaud, C., Dobler, A., Hodnebrog, Ø., Kartsios, S., Lenderink, G., de Vries, H., Göktürk, O., Milovac, J., Feldmann, H., Truhetz, H., Demory, M. E., Warrach-Sagi, K., Keuler, K., Adinolfi, M., Raffa, M., Tölle, M., Sieck, K., Bastin, S., and Soares, P. M. M.: The added value of simulated near-surface wind speed over the Alps from a km-scale multimodel ensemble, Clim. Dynam., https://doi.org/10.1007/s00382-024-07257-4, 2024.

Muñoz Sabater, J., Dutra, E., Agustí-Panareda, A., Albergel, C., Arduini, G., Balsamo, G., Boussetta, S., Choulga, M., Harrigan, S., Hersbach, H., Martens, B., Miralles, D. G., Piles, M., Rodríguez-Fernández, N. J., Zsoter, E., Buontempo, C., and Thépaut, J.-N.: ERA5-Land: a state-of-the-art global reanalysis dataset for land applications, Earth Syst. Sci. Data, 13, 4349–4383, https://doi.org/10.5194/essd-13-4349-2021, 2021.

Muñoz-Sabater, J., Dutra, E., Agustí-Panareda, A., Albergel, C., Arduini, G., Balsamo, G., Boussetta, S., Choulga, M., Harrigan, S., Hersbach, H., et al.: ERA5-Land: A state-of-the-art global reanalysis dataset for land applications, Earth Syst. Sci. Data, 13, 4349–4383, https://doi.org/10.5194/essd-13-4349-2021, 2021.

https://doi.org/10.5194/egusphere-2026-2517
Preprint. Discussion started: 11 June 2026

Nijsse, F. J., Cox, P., and Williamson, M. S.: Emergent constraints on transient climate response (TCR) and equilibrium climate sensitivity (ECS) from historical warming in CMIP5 and CMIP6 models, Earth Syst. Dynam., 11, 737–750, https://doi.org/10.5194/esd-11-737-2020, 2020.

O'Neill, B., Tebaldi, C., van Vuuren, D., Eyring, V., Friedlingstein, P.and Hurtt, G., Knutti, R.and Kriegler, E., Lamarque, J.-F., Lowe, J., Meehl, G., Moss, R., Riahi, K., and Sanderson, B.: The Scenario Model Intercomparison Project (ScenarioMIP) for CMIP6, Geosci. Model Dev., 9, 3461–3482, https://doi.org/10.5194/gmd-9-3461-2016, 2016.

Pan, B., Anderson, G. J., Goncalves, A., Lucas, D. D., Bonfils, C. J. W., Lee, J., Tian, Y., and Ma, H.-Y.: Learning to Correct Climate Projection Biases, J. Adv. Model. Earth Sy., 13, e2021MS002 509, https://doi.org/10.1029/2021MS002509, 2021.

Perkins, S. E., Pitman, A. J., Holbrook, N. J., and McAneney, J.: Evaluation of the AR4 climate models' simulated daily maximum temperature, minimum temperature, and precipitation over Australia using probability density functions, J. Climate, 20, 4356–4376, https://doi.org/10.1175/JCLI4253.1, 2007.

Pham, T. V., Steger, C., Rockel, B., Keuler, K., Kirchner, I., Mertens, M., Rieger, D., Zängl, G., and Früh, B.: ICON in Climate Limited-area Mode (ICON release version 2.6.1): a new regional climate model, Geoscientific Model Development, 14, 985–1005, https://doi.org/10.5194/gmd-14-985-2021, 2021.

Pichelli, E., Coppola, E., Sobolowski, S., Ban, N., Giorgi, F., Stocchi, P., Alias, A., Belušić, D., Berthou, S., Cardoso, R. M., Chan, S., Christensen, O. B., Dobler, A., de Vries, H., Goergen, K., Kendon, E. J., Keuler, K., Lenderink, G., Lorenz, T., Mishra, A. N., Panitz, H.-J., Schär, C., Soares, P. M. M., et al.: The first multi-model ensemble of regional climate simulations at kilometer-scale resolution part 2: historical and future simulations of precipitation, Clim. Dynam., 56, 3581–3602, https://doi.org/10.1007/s00382-021-05657-4, 2021.

Pietikäinen, J.-P., Sieck, K., Buntemeyer, L., Frisius, T., Nam, C., Hoffmann, P., Pop, C., Rechid, D., and Jacob, D.: REMO2020: a modernised modular regional climate model, Geosci. Model Dev., 18, 7907–7949, https://doi.org/10.5194/gmd-18-7907-2025, 2025.

Pinto, J. G., Hundhausen, M., Weber, A., Kohlhepp, R., Mihalyfi-Dean, C., Schipper, J. W., and Feldmann, H.: User-relevant climate indices and associated uncertainties from transient convection-permitting climate model projections, Int. J. Climatol., 46, https://doi.org/10.1002/joc.70304, 2026.

Pörtner, H.-O., Roberts, D., Tignor, M., Poloczanska, E., Mintenbeck, K., Alegría, A., Craig, M., Langsdorf, S., Löschke, S., Möller, V., Okem, A., and Rama, B., eds.: Climate Change 2022: Impacts, Adaptation and Vulnerability. Contribution of Working Group II to the Sixth Assessment Report of the Intergovernmental Panel on Climate Change, Cambridge University Press, Cambridge, UK and New York, NY, https://doi.org/10.1017/9781009325844, 2022.

Pörtner, H.-O., Roberts, D., Adams, H., Adler, C., Aldunce, P., Ali, E., Ara Begum, R., Betts, R., Bezner Kerr, R., Biesbroek, R., Birkmann, J., Bowen, K., Castellanos, E., Cissé, G., Constable, A., Cramer, W., Dodman, D., Eriksen, S., Fischlin, A., Garschagen, M., Gilmore, E., Glavovic, B., Haasnoot, M., Harper, S., Hasegawa, T., Hayward, B., Hirabayashi, Y., Howden, M., Kalaba, K., Kiessling, W., Lasco, R., Lawrence, J., Lemos, M., Lempert, R., Ley, D., Lissner, T., Lluch-Cota, S., Löschke, S., Lucatello, S., Luo, Y., Mackey, B., Moaharj, S., Mendez, C., Mintenbeck, K., Möller, V., Moncassim Vale, M., Morecroft, M., Mukherji, A., Mustonen, T., Mycoo, M., Nalau, J., Okem, A., Ometto, J., Parmesan, C., Pelling, M., Pinho, P., Poloczanska, E., Racault, M.-F., Reckien, D., Pereira, J., Revi, A., Rose, S., Sanchez-Rodriguez, R., Schipper, E., Schmidt, D., Schoeman, D., Shaw, R., Singh, C., Solecki, W., Stringer, L., Thomas, A., Totin, E., Trisos, C., van Aalst, M., Viner, D., Wairu, M., Warren, R., Yanda, P., and Zaiton Ibrahim, Z.: SPM - Summary for Policymakers, pp. 3–34, Cambridge University Press, United Kingdom, https://doi.org/10.1017/9781009325844.001, 2023.

https://doi.org/10.5194/egusphere-2026-2517
Preprint. Discussion started: 11 June 2026

Prein, A. F., Langhans, W., Fosser, G., Ferrone, A., Ban, N., Goergen, K., Keller, M., Tölle, M., Gutjahr, O., Feser, F., Brisson, E., Kollet, S., Schmidli, J., van Lipzig, N. P. M., and Leung, R.: A review on regional convection-permitting climate modeling: Demonstrations, prospects, and challenges, Rev. Geophys., 53, 323–361, https://doi.org/https://doi.org/10.1002/2014RG000475, 2015.

Prill, F., Reinert, D., Rieger, D., and Zaengel, G.: ICON Tutorial: Working with the ICON Model, Tech. rep., Deutscher Wetterdienst, Karlsruhe Institute of Technology, Max-Planck-Institut fuer Meteorologie, https://doi.org/10.5676/DWD_pub/nwv/icon_tutorial2023, 2023.

Rauthe, M., Steiner, H., Riediger, U., Mazurkiewicz, A., and Gratzki, A.: A Central European precipitation climatology – Part I: Generation and validation of a high-resolution gridded daily data set (HYRAS), Meteorol. Z., 22, 235–256, https://doi.org/10.1127/0941-2948/2013/0436, 2013.

Razafimaharo, C., Krähenmann, S., Höpp, S., Rauthe, M., and Deutschländer, T.: New high-resolution gridded dataset of daily mean, minimum, and maximum temperature and relative humidity for Central Europe (HYRAS), Theor. Appl. Climatol., 142, 1531–1553, 2020.

Reyers, M., Pinto, J. G., and Moemken, J.: Statistical-dynamical downscaling for wind energy potentials: evaluation and applications to decadal hindcasts and climate change projections, Int. J. Climatol., 35, 229–244, https://doi.org/10.1002/joc.3975, 2015.

Richling, A.: 2D-Blocking, Technical report, FU Berlin, https://gitlab.met.fu-berlin.de/tools4freva/blocking_2D, 2020.

Rockel, B. and Geyer, B.: COSMO-CLM Starter Package, https://doi.org/10.5281/zenodo.7290478, 2022a.

Rockel, B. and Geyer, B.: SPICE (Starter Package for ICON-CLM Experiments), https://doi.org/10.5281/zenodo.6838984, 2022b.

Rockel, B., Will, A., and Hense, A.: The Regional Climate Model COSMO-CLM (CCLM), Meteorol. Z., 17, 347–348, https://doi.org/10.1127/0941-2948/2008/0309, 2008.

Rousi, E., Fink, A. H., Andersen, L. S., Becker, F. N., Beobide-Arsuaga, G., Breil, M., Cozzi, G., Heinke, J., Jach, L., Niermann, D., Petrovic, D., Richling, A., Riebold, J., Steidl, S., Suarez-Gutierrez, L., Tradowsky, J. S., Coumou, D., Düsterhus, A., Ellsäßer, F., Fragkoulidis, G., Gliksman, D., Handorf, D., Haustein, K., Kornhuber, K., Kunstmann, H., Pinto, J. G., Warrach-Sagi, K., and Xoplaki, E.: The extremely hot and dry 2018 summer in central and northern Europe from a multi-faceted weather and climate perspective, Nat. Hazards Earth Syst. Sci., 23, 1699–1718, https://doi.org/10.5194/nhess-23-1699-2023, 2023.

Schär, C., Ban, N., Corti, S., and et al.: Kilometer-scale climate models: Prospects and challenges, Nat. Clim. Change, 10, 799–808, https://doi.org/10.1038/s41558-020-00944-6, 2020.

Schartner, T.: Circulation Weather Types (CWT), Technical report, FU Berlin, https://gitlab.dkrz.de/freva/plugins4freva/cwt, 2016.

Schulzweida, U.: CDO User Guide, https://doi.org/10.5281/zenodo.7112925, 2022.

Schupfner, M., Wieners, K.-H., Wachsmann, F., Steger, C., Bittner, M., Jungclaus, J., Früh, B., Pankatz, K., Giorgetta, M., Reick, C., Legutke, S., Esch, M., Gayler, V., Haak, H., de Vrese, P., Raddatz, T., Mauritsen, T., von Storch, J.-S., Behrens, J., Brovkin, V., Claussen, M., Crueger, T., Fast, I., Fiedler, S., Hagemann, S., Hohenegger, C., Jahns, T., Kloster, S., Kinne, S., Lasslop, G., Kornblueh, L., Marotzke, J., Matei, D., Meraner, K., Mikolajewicz, U., Modali, K., Müller, W., Nabel, J., Notz, D., Peters-von Gehlen, K., Pincus, R., Pohlmann, H., Pongratz, J., Rast, S., Schmidt, H., Schnur, R., Schulzweida, U., Six, K., Stevens, B., Voigt, A., and Roeckner, E.: DKRZ MPI-ESM1.2-HR model output prepared for CMIP6 ScenarioMIP ssp370, https://doi.org/10.22033/ESGF/CMIP6.4399, 2019.

Shiogama, H., Abe, M., and Tatebe, H.: MIROC MIROC6 model output prepared for CMIP6 ScenarioMIP ssp370, https://doi.org/10.22033/ESGF/CMIP6.5752, 2019.

Sieck, K., Pinto, J. G., Geyer, B., Keuler, K., Beier, C., Braun, C., Ehmele, F., Feldmann, H., Frisius, T., Heinrich, P., Hundhausen, M., Petrik, R., and Trachte, K.: NUKLEUS - A First Kilometer Scale Multi-model Climate Ensemble for Germany: Evaluation, submitted to Geosci. Model Dev., 2026.

https://doi.org/10.5194/egusphere-2026-2517
Preprint. Discussion started: 11 June 2026

Smith, C., Nicholls, Z., Armour, K., Collins, W., Forster, P., Meinshausen, M., Palmer, M., and Watanabe, M.: The Earth's Energy Budget, Climate Feedbacks, and Climate Sensitivity Supplementary Material, in *Climate Change 2021: The Physical Science Basis. Contribution of Working Group I to the Sixth Assessment Report of the Intergovernmental Panel on Climate Change* [Masson-Delmotte, V., Zhai, P., Pirani, A., Connors, S.L., Péan, C., Berger, S., Caud, N., Chen, Y., Goldfarb, L., Gomis, M.I., Huang, M., Leitzell, K., Lonnoy, E., Matthews, J.B.R., Maycock, T.K., Waterfield, T., Yelekçi, O., Yu, R., and Zhou, B. (eds.)]. Available from https://www.ipcc.ch/report/ar6/wg1/downloads/report/IPCC_AR6_WGI_Chapter07_SM.pdf, last access: 10 February 2026, 2021.

Soares, P. M. M., Careto, J. A. M., Cardoso, R. M., Goergen, K., Katragkou, E., Sobolowski, S., Coppola, E., Ban, N., Belušić, D., Berthou, S., Caillaud, C., Dobler, A., Hodnebrog, Ø., Kartsios, S., Lenderink, G., Lorenz, T., Milovac, J., Feldmann, H., Pichelli, E., Truhetz, H., Demory, M. E., de Vries, H., Warrach-Sagi, K., Keuler, K., Raffa, M., Tölle, M., Sieck, K., and Bastin, S.: The added value of km-scale simulations to describe temperature over complex orography: the CORDEX FPS-Convection multi-model ensemble runs over the Alps, Clim. Dynam., 62, 4491–4514, https://doi.org/10.1007/s00382-022-06593-7, 2024.

Sobolowski, S., Somot, S., Fernandez, J., Evin, G., Maraun, D., Kotlarski, S., Jury, M., Benestad, R., Teichmann, C., Christensen, O., Bülow, K., Buonomo, E., Katragkou, E., Steger, C., Sørland, S., Nikulin, G., McSweeney, C., Dobler, A., Palmer, T., Wilke, R., Boé, J., Brunner, L., Ribes, A., Qasmi, S., Nabat, P., Sevault, F., Oudar, T., and Brands, S.: TEURO-CORDEX CMIP6 GCM Selection & Ensemble Design: Best Practices and Recommendations, Tech. rep., EURO-CORDEX, https://doi.org/10.5281/zenodo.7673400, 2023.

Sørland, S. L., Brogli, R., Pothapakula, P. K., Russo, E., Van de Walle, J., Ahrens, B., Anders, I., Bucchignani, E., Davin, E. L., Demory, M.-E., Dosio, A., Feldmann, H., Früh, B., Geyer, B., Keuler, K., Lee, D., Li, D., van Lipzig, N. P. M., Min, S.-K., Panitz, H.-J., Rockel, B., Schär, C., Steger, C., and Thiery, W.: COSMO-CLM regional climate simulations in the Coordinated Regional Climate Downscaling Experiment (CORDEX) framework: a review, Geoscientific Model Development, 14, 5125–5154, https://doi.org/10.5194/gmd-14-5125-2021, 2021.

Steger, C. and Bucchignani, E.: Regional Climate Modelling with COSMO-CLM: History and Perspectives, Atmosphere, 11, 1250, https://doi.org/10.3390/atmos11111250, 2020.

Stevens, B., Satoh, M., Auger, L., Biercamp, J., Bretherton, C. S., Chen, X., Düben, P., Judt, F., Khairoutdinov, M., Klocke, D., Kodama, C., Kornblueh, L., Lin, S.-J., Neumann, P., Putman, W. M., Röber, N., Shibuya, R., Vanniere, B., Vidale, P. L., Wedi, N., and Zhou, L.: DYAMOND: the DYnamics of the Atmospheric general circulation Modeled On Non-hydrostatic Domains, Progress in Earth and Planetary Science, 6, 61, https://doi.org/10.1186/s40645-019-0304-z, 2019.

Stevens, B., Acquistapace, C., Hansen, A., Heinze, R., Klinger, C., Klocke, D., Rybka, H., Schubotz, W., Windmiller, J., Adamidis, P., et al.: The added value of large-eddy and storm-resolving models for simulating clouds and precipitation, Journal of the Meteorological Society of Japan. Ser. II, 98, 395–435, https://doi.org/10.2151/jmsj.2020-021, 2020.

Tatebe, H. and Watanabe, M.: MIROC MIROC6 model output prepared for CMIP6 CMIP historical, https://doi.org/10.22033/ESGF/CMIP6.5603, 2018.

Tiedtke, M.: A comprehensive mass flux scheme for cumulus parameterization in large-scale models, Mon. Weather Rev., 117, 1779–1800, https://doi.org/10.1175/1520-0493(1989)117<1779: ACMFSF>2.0.CO;2, 1989.

Vautard, R., Kadygrov, N., Iles, C., Boberg, F., Buonomo, E., Bülow, K., Coppola, E., Corre, L., van Meijgaard, E., Nogherotto, R., Sandstad, M., Schwingshackl, C., Somot, S., Aalbers, E., Christensen, O. B., Ciarlo, J. M., Demory, M.-E., Giorgi, F., Jacob, D., Jones, R. G., Keuler, K., Kjellström, E., Lenderink, G., Levavasseur, G., Nikulin, G., Sillmann, J., Solidoro, C., Sørland, S. L., Steger, C., Teichmann, C., Warrach-Sagi, K., and Wulfmeyer, V.: Evaluation of the Large EURO-CORDEX Regional Climate Model Ensemble, Journal of Geophysical Research: Atmospheres, 126, e2019JD032 344, https://doi.org/10.1029/2019JD032344, 2021.

https://doi.org/10.5194/egusphere-2026-2517
Preprint. Discussion started: 11 June 2026

Voit, P., Hundhausen, M., Seregina, L., Feldmann, H., Ahrens, B., and Heistermann, M.: Southern Germany's 100-year flash flood discharge expected to increase by 30 % under an RCP8.5 climate, EGUsphere, 2026, 1–16, https://doi.org/10.5194/egusphere-2026-1229, 2026.

Vrac, M. and Friederichs, P.: Multivariate—Intervariable, Spatial, and Temporal—Bias Correction, J. Climate, 28, 218–237, https://doi.org/10.1175/JCLI-D-14-00059.1, 2015.

World Meteorological Organization: WMO guidelines on the calculation of climate normals (WMO-No, 1203), WMO, Geneva, Switzerland, https://library.wmo.int/idurl/4/55797, 2017.

Zaengl, G., Reinert, D., Ripodas, P., and Baldauf, M.: The ICON (ICOsahedral Non-hydrostatic) modelling framework of DWD and MPI-M: Description of the non-hydrostatic dynamical core, Q. J. R. Meteorol. Soc., 141, 563–579, https://doi.org/10.1002/qj.2378, 2015.